

**Nikolajs Glīzde**

# **DEVELOPMENT OF REMOTELY PILOTED AIRCRAFT SYSTEM WITH EXTENDED ENDURANCE**

Summary of the Doctoral Thesis



**RIGA TECHNICAL UNIVERSITY**  
Faculty of Mechanical Engineering, Transport and Aeronautics  
Institute of Aeronautics

**Nikolajs Glīzde**  
Doctoral Student of the Study Program “Transport”

**DEVELOPMENT OF REMOTELY PILOTED  
AIRCRAFT SYSTEM WITH EXTENDED  
ENDURANCE**

**Summary of the Doctoral Thesis**

Scientific supervisor  
Associate Professor Dr. sc. ing.  
**MĀRIS HAUKA**

RTU Press  
Riga 2023

Glīzde, N. Development of Remotely Piloted Aircraft System with Extended Endurance. Summary of the Doctoral Thesis. Riga: RTU Press, 2023. – 55 p.

Published in accordance with the decision of the Promotion Council “RTU P-22” of 1 December 2023, Minutes No. 04030-9/16.1/11.

Cover picture by Nikolajs Glīzde

<https://doi.org/10.7250/9789934370168>  
ISBN 978-9934-37-016-8 (pdf)

# **DOCTORAL THESIS PROPOSED TO RIGA TECHNICAL UNIVERSITY FOR THE PROMOTION TO THE SCIENTIFIC DEGREE OF DOCTOR OF SCIENCE**

To be granted the scientific degree of Doctor of Science (Ph. D.), the present Doctoral Thesis has been submitted for defence at the open meeting of RTU Promotion Council on January 12, 2024, at the Institute of Aeronautics of Faculty of Mechanical Sciences, Transport and of Riga Technical University, 6B Ķīpsālas Street, Room 513.

## **OFFICIAL REVIEWERS**

Associate Professor Dr. sc. ing. Ali Arshad  
Riga Technical University

Professor Dr. sc. ing. Rafal Chatys  
Technical University of Kielce, Poland

Professor Dr. habil. sc. ing. Krzysztof Szafran  
Institute of Aviation, Poland

## **DECLARATION OF ACADEMIC INTEGRITY**

I hereby declare that the Doctoral Thesis submitted for review to Riga Technical University for promotion to the scientific degree of Doctor of Science (Ph. D.) is my own. I confirm that this Doctoral Thesis has not been submitted to any other university for promotion to a scientific degree.

Nikolajs Glīzde ..... (signature)

Date: .....

The Doctoral Thesis has been written in Latvian. It consists of an Introduction, 8 chapters, Conclusions, 61 figures, 47 tables, and 22 appendices; the total number of pages is 156, not including appendices. The Bibliography contains 62 titles.

## NOMENCLATURE

*AGL – Above Ground Level*  
*ALR – Automatic Launch and Recovery*  
*AR – Aspect Ratio (span/reference area, applied to wings and tails)*  
*ASL – Above Sea Level*  
*UAS – Unmanned Aircraft System*  
*CAD – Computer-Aided Design*  
*CFD – Computational Fluid Dynamics*  
 *$C_L$  – Wing Lift Coefficient*  
 *$C_{L\text{-design}}$  – Wing Design Lift Coefficient*  
*COTS – Commercial Off-The-Shelf*  
*EO – Electro-Optical*  
 *$f$  – fuselage fineness ratio = length/diameter*  
*GA – Genetic Algorithm*  
*GCS – Ground Control Station*  
*GPS – Global Positioning System*  
*HLD – High Lift Device*  
*ICAO – International Civil Aviation Organisation*  
*IR – Infra-Red*  
*ISR – Intelligence, Surveillance, Reconnaissance*  
*L/D – Lift-to-Drag Ratio*  
*LE – Leading Edge (wing or tail)*  
*M – Mach Number*  
*MDO – Multidisciplinary Optimization*  
*MOM – Measure of Merit (Objective Function in Optimization)*  
*NDV – Net Design Volume*  
*P/W – Power-to-weight ratio of aircraft*  
*RPV – Remotely Piloted Vehicles*  
*SUAV – Small Unmanned Aerial Vehicle*  
 *$t/c$  – airfoil thickness/chord length*  
*T/W – Thrust-to-weight ratio*  
*TE – Trailing Edge (wing or tail)*  
*UAV – Unmanned/Uninhabited Aerial Vehicle*  
*VAS ES – abbreviation in Latvian of State Joint-Stock company “Electronic Communications”*  
*W/S – Wing loading (weight/area)*

# CONTENTS

NOMENCLATURE .....	4
CONTENTS .....	5
1. CLASSIFICATION OF UNMANNED VEHICLE SYSTEMS, HIERARCHICAL SCHEME AND PRINCIPLE OF DEVELOPMENT .....	11
1.1. Categorization of systems .....	11
1.2. Hierarchical scheme of unmanned system.....	11
1.3. Development principle of unmanned system.....	12
1.4. Chapter summary and conclusions.....	16
2. CONCEPTUAL DESIGN PHASE.....	16
2.1. Selection of unmanned aerial vehicle type .....	16
2.2. Chapter summary and conclusions.....	19
3. PRIMARY CONSTRUCTION PHASE .....	20
3.1. Maximum take-off weight (MTOW) of aircraft .....	20
3.2. Construction of the UAS aircraft flight envelope .....	22
3.3. Chapter summary and conclusions.....	22
4. DETAIL CONSTRUCTION PHASE.....	24
4.1. Wing construction .....	24
4.2. Winglet design parameters calculation.....	24
4.3. The wing parameter optimization calculation.....	25
4.4. Selection and calculation of landing system.....	26
4.5. Innovative take-off system selection and calculation.....	28
4.6. Engine system selection and calculation .....	31
4.7. Battery selection.....	32
4.8. Selection of avionics components .....	33
4.9. Aircraft body construction .....	34
4.10. Selection of ground control station.....	34
4.11. Design and selection of payload element.....	35
4.12. Chapter summary and conclusions .....	36
5. TESTING THE DEVELOPMENT OF AN UNMANNED AERIAL VEHICLE SYSTEM .....	37
5.1. Optimization of the flight parameters of an unmanned aircraft.....	37
5.2. Unmanned aerial vehicle system aircraft optimization .....	40
5.3. Chapter summary and conclusions.....	40
6. UNMANNED AIRCRAFT EXPERIMENTAL MODEL.....	41
6.1. Drone experimental model flight parameters.....	41
6.2. Conceptual and experimental drone model dimensional analysis.....	42

6.3. Scaled experimental model test un parameter identification in the wind tunnel .....	46
6.4. Chapter summary and conclusions.....	48
RECOMMENDATIONS FOR FURTHER RESEARCH .....	49
CONCLUSIONS .....	51
BIBLIOGRAPHY .....	52

## **THE AIM AND TASKS OF THE THESIS**

### **The aim of the Thesis**

The Thesis aims to develop an unmanned aerial vehicle system (UAS) with increased flight duration and a new type of landing system.

### **Tasks of the Thesis**

1. Analysis of studies carried out so far in the field of mini-UAV systems.
2. Analysis and selection of the most appropriate design selection procedure for the conceptual UAV model.
3. Development of the conceptual aircraft model of the UAV and selection of other elements of the system according to the developed procedure.
4. Experimental flights to research the development of new take-off and landing systems.
5. Computer simulation of the developed aircraft model for the performance assessment.
6. Dimensional analysis of the conceptual and experimental UAV models.

## **RESEARCH METHODS**

Methodology of parts of the research carried out and the research methods used:

- Analysis of literature sources.
- Technical calculations in MATLAB.
- C/C ++ programming language used for programming.
- Multi-disciplinary optimization has been used to obtain the best parameter values.
- Simulation of developed systems in a computer program.
- Processing and modelling of experimental testing data in a computer program.

## **RESEARCH OBJECTS**

- Remotely controlled aircraft.
- Remotely controlled aircraft avionics/avionics systems.
- Remotely controlled aircraft take-off and landing systems.
- Battery systems.
- Electric motor systems.
- Computer simulation programs.

## **SCIENTIFIC NOVELTY OF RESEARCH**

Innovative solutions developed as a result of the promotion work:

- The technical and economic advantages of a proven flying wing-type drone aerodynamic scheme in the mini-UAV category represented in terms of the small number of the components to be used and innovative take-off and landing systems.

- The development of a new design technique for the flight envelope chart based on the MATLAB program for aircraft design calculations.
- A new system for calculation of the engine power and the wing reference area required for an aircraft in aircraft design calculations has been developed based on the matching plot technique in the MATLAB program.
- Demonstrated positive effects of drone wing winglets on flying wing aerodynamic parameters in small Reynolds numbers.
- A new type of UAV landing has been reviewed, based on the aerodynamic characteristics of the flying wing-type unmanned aerial vehicle, providing a landing capability in a restricted free area, a reduced impact load at the moment of landing, as well as a reduced system total weight, as no additional equipment is required to implement the landing process.
- A new method of launching an UAS aircraft has been reviewed based on the aerodynamic properties of a flying wing-type drone, which ensures the launch of hand-launched drones taking into account the operator's safety, the possibility of launching in a restricted free area, as well as a lesser overall weight of the system, as no additional heavy equipment such as the launch catapult is required for the implementation of the launch process.

The results of the Thesis research will serve as evidence that the development of UAV systems, as well as the development of other systems, requires a systemic approach which makes it possible to fully assess the construction progress, find new solutions and assess their compliance with the requirements set. In the design of the model, a systemic approach allows for the use of freely commercially available components so that the cost of the system is economically advantageous for users engaged in environmental protection, nature monitoring and other similar functions, while not reducing the overall functionality of the system that is imposed by the design requirements.

By developing the results of the Thesis research, it will be possible to use them in all sectors using unmanned aerial vehicle systems, such as reconnaissance, surveillance, nature research, and pollution monitoring, allowing the choice of the required take-off or landing of the aircraft depending on the circumstances.

## **THESES TO BE DEFENDED**

- The simulation necessity for the UAV system under development.
- A new landing method for the system aircraft and its usefulness.
- A new launch method for the system aircraft and its usefulness.

## **PRACTICAL SIGNIFICANCE OF THE THESIS**

In the Thesis, a brand-new UAV system has been developed with improved performance characteristics and a new launch and landing system that has a significant impact on its

performance. The aircraft performance characteristics are better. The design of the unmanned aerial vehicle system uses freely commercially available components so that the cost of the system is economically advantageous for users engaged in environmental protection, nature monitoring and other similar functions, while not reducing the overall functionality of the system that is imposed by the design requirements at the start of construction.

The results of the Thesis can be used in aeronautics, navigation, surveillance, control, etc.

## **APPROBATION OF THE THESIS**

### **The research results were reported at 7 international scientific conferences**

1. 19th International Scientific Conference “Engineering for Rural Development 2020”, report “Remotely piloted aircraft system air vehicle wing airfoil selection,” N. Glizde, M. Urbach.
2. 18th International Scientific Conference “Engineering for Rural Development 2019”, report “Remotely piloted aircraft system air vehicle type selection,” N. Glizde, M. Urbach.
3. 22nd International Scientific Conference “Transport Means 2018,” Lithuania, 03–05.10.2018, report “Flight optimization for remotely piloted aircraft,” N. Glizde, M. Urbach.
4. RTU 58th International Scientific Conference, Latvia. 12–15.10.2017, report “Unmanned aircraft system air vehicle wing airfoil selection and planform design,” N. Glizde.
5. RTU 57th International Scientific Conference, Latvia. 14–18.10.2016, report “Identification and avoidance system for unmanned aerial vehicles,” N. Glizde.
6. RTU 57th International Scientific Conference, Latvia. 14–18.10.2016, “Unmanned aircraft system for military tasks,” N. Glizde.
7. 56th International Scientific Conference of the RTU, Latvia. 14–16.10.2015, report “Trends in the future of unmanned aircraft in the world,” N. Glizde.

### **The research results were presented in five scientific articles**

1. Glizde, N., Urbaha, M (2020), remotely piloted aircraft system air vehicle wing airfoil selection. In: Proceedings of International Scientific Conference “Engineering for Rural Development 2020”, Latvia, Jelgava, 20–22 May 2020, pp. 1522–1530. ISSN 1691-5976. SOURCE: Elsevier SCOPUS. TF379.
2. Glizde, N., Urbaha, M. (2019), remotely piloted aircraft system air vehicle type selection. In: Proceedings of International Scientific Conference “Engineering for Rural Development 2019”, Latvia, Jelgava, 22–24 May 2019, pp. 1302–1312. SOURCE: Elsevier SCOPUS. DOI: 10.22616/ERDev2019.18. N241.
3. Glizde, N., Urbaha, M. (2018), flight optimization for remotely piloted aircraft. In: Transport Means 2018: Proceedings of the 22nd International Scientific Conference, Lithuania, mad, 03–06 October 2018. Shame: Shame University of Technology, Part III, pp. 1178–1184. ISSN 1822-296 X (Print), ISSN 2351-7034 (Online). SOURCE: SCOPUS.

4. Glizde, N. (2017), Wing and engine sizing by using the matching plot technique. – Transport and Aerospace Engineering, vol. 4, pp. 80–87, ISSN 2255-9876 (Online), ISSN 2255-968X (Print). Doi: 10.1515/tae-2017-0010, Source: de Gruyter.
5. Glizde, N. (2017), Plotting the flight envelop of an unmanned aircraft system Air vehicle. - Transport and Aerospace Engineering, vol. 5, pp. 48–59, ISSN 2255-9876 (Online), ISSN 2255-968X (Print). Doi: 10.1515/tae-2017-0018, Source: de Gruyter.

# 1. CLASSIFICATION OF UNMANNED VEHICLE SYSTEMS, HIERARCHICAL SCHEME AND PRINCIPLE OF DEVELOPMENT

## 1.1. Categorization of systems

Unmanned aerial vehicle systems can be classified by type and flight altitude and distance [6], [8], [9]. Separately military classification of UAS can be observed that is shown in Table 1.1 [8; 9].

Table 1.1

UAS classification [3]

Class	Category	Usage	Operation altitude	Operation radius	Primary support Commander	Example system
Class I (< 150 kg)	MICRO < 2 kg	Tactical groups, Individual (one operator)	Until 60 m AGL	5 km (LOS)	Group	Black Widow
	MINI 2-20 kg	Tactical subunit (manual launch)	Until 900 m AGL	25 km (LOS)	Platoon/Company	Scan Eagle, Skylark, Raven, DH3, Aladin, Strix
	SMAL >20 kg	Tactical unit (launch system)	Until 1 500 m AGL	50 km (LOS)	Battalion/ Brigade	Luna, Hermes 90
Class II (from 150 kg to 600 kg)	TACTICAL	Tactical structure	Until 3 000 m AGL	200 km (LOS)	Brigade	Sperwer, Iview 250, Hermes 450, Aerostar, Ranger
Class III (above 600 kg)	MALE	In operational zone	Until 13 700 m ASL	Unlimited (BLOS)	Allied tactical forces	Predator B, Predator A, Heron, Heron TP, Hermes 900
	HALE	Strategic / National	Until 19 800 m	Unlimited (BLOS)	In operational zone	Global Hawk
	Assault / Combat	Strategic / National	Until 19 800 m	Unlimited (BLOS)	In operational zone	Sentinel

Also, separately JARUS unmanned system classification can be reviewed [11-13]. JARUS consists of 65 organizations, 63 countries as well as EASA and EUROCONTROL.

## 1.2. Hierarchical scheme of unmanned system

The hierarchical scheme of unmanned system is shown in Fig.1.1. [8], [9].

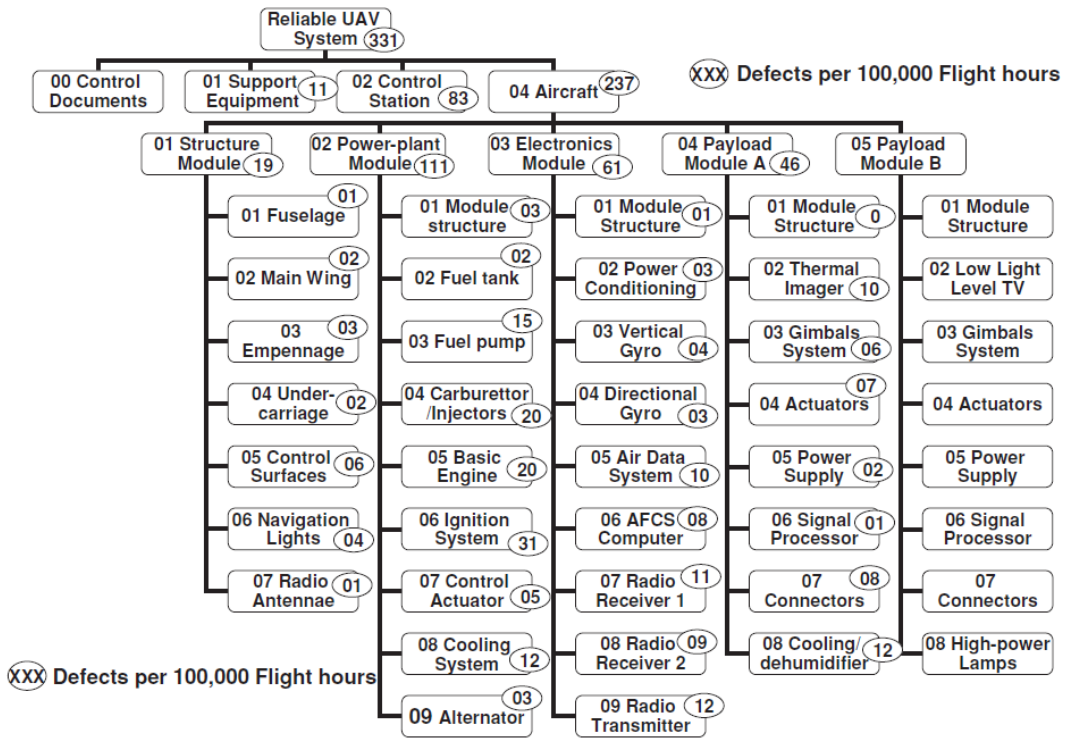


Fig.1.1. Unmanned system hierarchical model [8].

### 1.3. Development principle of unmanned system

Most aircraft-based systems are developed in three phases:

- conceptual phase;
- primary development phase;
- detail development phase.

The remaining phases follow after the development of the initial model. These include the development of modifications during model development and subsequent modifications or improvements during the use by the system user [14], [15].

The requirements of UAV system for development are drawn up in Table 1.2. Farther calculations [14-17] are completed based on data in Table 1.2.

Table 1.2

## Design requirements for the system under development

No.	Characteristic	Requirement	Desired value	Desired technical features
1.	UAV mass – ready for launch	max 9 kg	6 - 8 kg	Made from light, strong material that provides structure durability under loads, resilience to moist (possibly carbon fibre material).
2.	Drive	Electric motor	-	Electric motor with control unit.
3.	Endurance	300 min	> 300 min	Rechargeable batteries that provide necessary flight endurance.
4.	Appropriate flight altitude	> 300 m	350 m or altitude that provides stealthy usage	The flight altitude that provides stealthy usage is 300 m. The flight altitude that with good data transfer and at least 300 min flight endurance should be provided.
5.	Launch altitude	< 4 000 m	-	ASL
6.	Operational range	until 50 km	50 – 75 km	Data terminal with appropriate antenna that provides necessary transmission range.
7.	Payload	EO/IR camera	One gimbaled system	Payload that is operational during day and night time, weighing from 200 to 400 g.
8.	The UAS air vehicle should be dismountable, collapsable and carriable in backpack	Composing time: < 10 min (ready for launch)	-	-
9.	Launching system	manual	manual	As an option the launching catapult system should be envisaged in the set.
10.	Landing	Can be set automatic on the airframe or with chute	-	Autopilot system.
11.	Command and control	Ground control station, portable, < 10 kg.	-	Ready to use ground control station, carriable in backpack, or made from appropriate components.
12.	Usable temperature range	-15°C ÷ +40°C	-20°C ÷ +60°C	Depends on the usable temperature range of separate components.

This section describes the design process of the UAV system according to the systems engineering approach applied and gives a diagram of the system to be developed.

According to the calculation, the UAS should provide communication up to a distance of ~ 70 km in the line of direct vision (*LOS*). The communication quality varies depending on the frequency range used. There are systems where the same frequency range is used for both aircraft data transmission and payload data transmission. The transmission of payload data should use a higher frequency range due to the large amount of data. The communication quality check was performed on the *Radio Mobile* program. The selected ranges of potential communications and the resulting data are summarized in Table 1.3 [8], [18], [19].

Table 1.3

Radio Test Result on *Radio Mobile*

No.	Frequency range, MHz	Power, W	Communication distance, km	Communication quality, %
1	869.4–869.65	2	63	40
		4	90	85
		6	90	95
2	2 400–2 483.5	2	105	-
		4	104	30
		6	105	60
		8	106	80
		10	106	90

The summary of system development, the conceptual, initial, detailed design part and production and/or construction is referred to as *the acquisition stage*. The summary of the product use, support, transition and release parts for the use stage are presented in Fig. 1.2. Aircraft constructors need to be careful about the results of the use at an early stage of construction and development. They should also conduct the product life cycle engineering research at an early stage of the construction process.

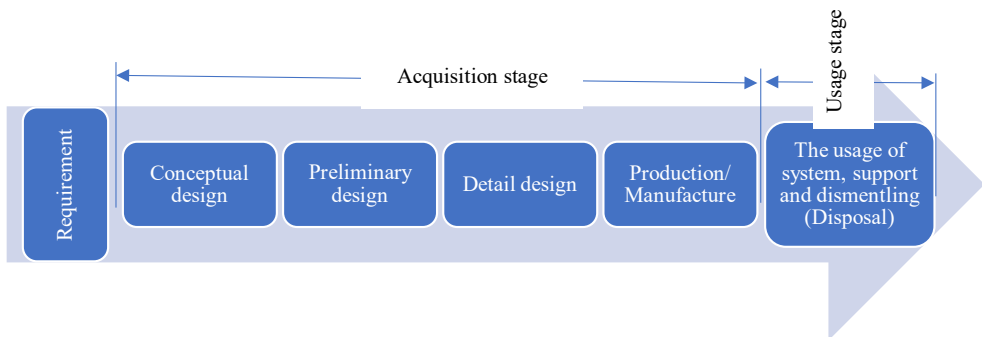


Fig.1.2. The life cycle model of the system [14; 20].

Fig. 1.3 shows the relationship between the main design measures in the system engineering approach. The design process started with the conceptual design phase based on design requirements. The initial design phase started immediately after the conceptual design phase and uses the results from the conceptual design phase.

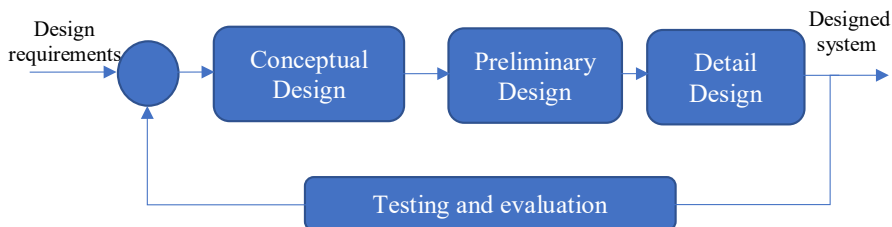


Fig.1.3. The connection between four main design stages [14; 20].

At the beginning of the conceptual design, the technical measures (*TPM*) of the system to be developed, describing the performance requirements of the system, shall be determined. Technical dimensions shall include qualitative and quantitative factors such as customer complaint, human factor, weight, geometry, volume, speed, process duration, operational costs, maintenance costs, identifiability, production opportunities, and obtainability.

Accordingly, a breakdown of the system into subsystems is drawn up according to Table 1.2 of the construction requirements, that is shown Fig. 1.4.

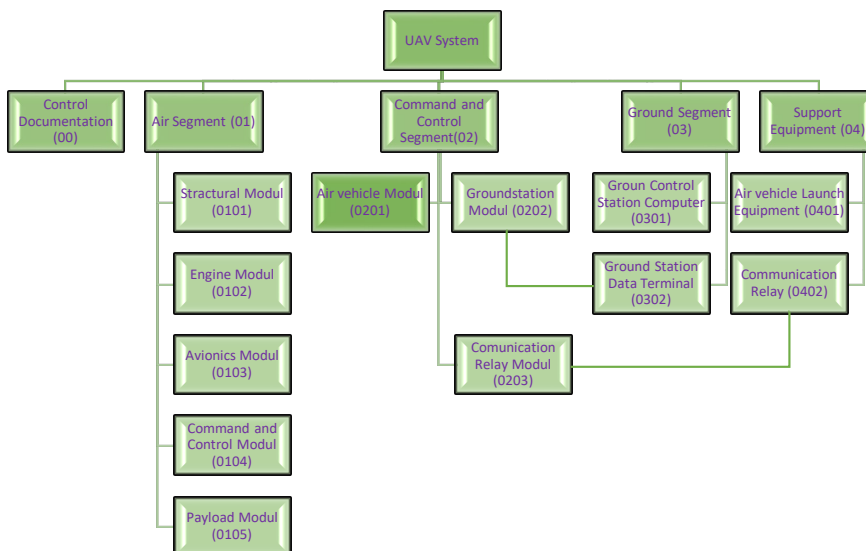


Fig.1.4. UAV system hierarchical model [20 – 25].

According to the UAV hierarchical model, the design or selection of system elements from those in production is carried out using the multidisciplinary optimization method [13]–[20].

## 1.4. Chapter summary and conclusions

In this chapter, globally adopted classification of UAV systems is reviewed. This made it possible to better understand the diversity and performance of the systems in production, the areas of their use and the payloads used on those systems.

This section closer reviews the structure of the UAV, its lifecycle maintenance process and the system for ensuring the maintenance process. Also, UAV properties that influence their covert use were considered, which gave more detailed understanding of the characteristics of the electromagnetic spectrum and the methods by which a reduction of each electromagnetic spectrum can be achieved in order to prevent its detection, both for the purposes of covert use, when the UAVs are used for specific military or internal affairs purposes, or when used in the field for nature observation, not to interfere with living nature.

In this chapter the design process of the UAS was reviewed. Also, the steps in the design process were reviewed. It was examined how to properly organise the construction process in order to be able to track its progress and avoid errors that could cause problems in further phases of the design. It was considered how to draw up correctly the system structural diagram for the construction process, the workflow schedule, as well as the financial flow schedule that is a very necessary thing for construction of the real system in strict terms.

## 2. CONCEPTUAL DESIGN PHASE

### 2.1. Selection of unmanned aerial vehicle type

Using the system engineering approach method, step by step optimal UAV type is selected to achieve the design objectives in accordance with the requirements [14], [15], [26]–[29]. UAV type is selected in 5 steps.

Step 1. Sets out a list of possible UAV configurations of which A is the basic configuration [14], [15] and further describes the B, C, D, E, F, G, and H configurations.

Step 2. Defines the technical performance measures (*TPM*) that include system design requirements. *TPM* parameters shall include both qualitative and quantitative data, human factors, weight, geometric shape, volume, speed, process duration, operational costs, maintenance costs, identifiability, production opportunities, and obtainability [14], [28], [31].

Step 3. Defines the quantitative size of the evaluation criteria and its priority. The focus should be on the performance, stability and controllability requirements of the aircraft [14], [32]. The design process shall determine the type of aircraft with its full technical specification. If the aircraft type is correctly determined, the further design process will be easier and will help avoid misunderstandings in future design phases. The aircraft type depends on the operational tasks and design requirements [14], [15], [17].

Step 4. The methodology used makes it possible to assess the characteristics of the systems by comparing several constructions quantitatively. To be sure that the selected configuration is the configuration that was searched for during this phase, you must follow the correct

methodology and calculation procedure. Each parameter is evaluated by 0 and 1. Priority weighted values are distributed among all measures of technical performance in such a way that they amount to 100 % [14], [15], [17], [31], [32]. Ten target parameters are defined. The index of each target parameter equals the investment amount of configuration parameters. Of the ten target design parameters, three have to be minimized: cost, weight and construction time.

The other design target parameters shall be maximized and they are: performance, flying quality, appearance, maintenance, manufacturing, dismantling and stealth.

Priorities for the target parameters of the construction to be minimized:

$$P_{\min} = P_C + P_W + P_T. \quad (2.1)$$

Priorities for the target parameters of the construction to be maximized:

$$P_{\max} = P_P + P_F + P_B + P_M + P_R + P_D + P_S. \quad (2.2)$$

The sum of design priority values should be minimized to 20 % and maximized to 80 %.

It can be seen from the Eqs. (2.1) and (2.2) that there are two values that determine the optimum design. These are  $DI_{\min}$  and  $DI_{\max}$ . In this case, when the  $P_{\max}$  variable is greater than  $P_{\min}$ , from the determined priorities and their respective weighted values, the configuration for which the  $DI_{\max}$  construction index is the largest will be selected for further construction as the optimum configuration [14], [31], [32].

Step 5. The results of the previous calculation that selects the optimum UAV configuration. Taking into consideration the above types of aircraft configurations, configuration alternatives and design target parameters, an evaluation table [14], [31]–[36] is drawn up.

Table 2.1 shows the sum values of the construction index  $DI_{\max}$  [26], [27].

Table 2.1

Design parameters table

No.	Configuration parameters ( $x_{Ci}$ )	Air vehicle configuration							
		A	B	C	D	E	F	G	H
1.	Construction:	-	-	-	-	-	-	-	-
	- conventional	-2	0	-2	-	-	-	-	-
	- non-conventional	-	-	-	7	4	3	4	4
2.	Engine:	-	-	-	-	-	-	-	-
	- electric motor	-5	-5	-5	7	1	1	3	3
3.	Engine number:	-	-	-	-	-	-	-	-
	- one	-	-4	-4	4	-2	-2	-2	-2
	- two	-3	-	-	-	-	-	-	-
4.	Engine placement:	-	-	-	-	-	-	-	-
	- on wings	4	-	-	-	-	-	-	-
	- airframe front	-	-3	-	-	-	-	-	-
	- airframe aft	-	-	-	8	8	8	8	8
	- airframe midle	-	-	-11	-	-	-	-	-
5.	Wings:	-	-	-	-	-	-	-	-
	wing number:	-	-	-	-	-	-	-	-

	- one	1	1	1	4	2	2	4	4
	wing shape:	-	-	-	-	-	-	-	-
	- rectangular	-3	-	-	-	-	-	-	-
	- tapered	-	-5	-6	10	1	1	-1	-2
	- elliptic	-	-	-	-	-	-	2	7
	- defined back sweep	-	1	0	2	2	2	0	1
	- defined dihedral	-1	0	0	1	2	2	-1	-1
	Wing placement:	-	-	-	-	-	-	-	-
	- mid	-	-	-	8	8	8	-	-
	- high	1	1	-	-	-	-	1	1
	- parasol	-	-	-3	-	-	-	-	-
6.	Tail:	-	-	-	-	-	-	-	-
	- conventional	7	7	5	-	-	-	-	-
	- non-conventional	-	-	-	-	-	-	4	6
	horizontal tail:	-	-	-	-	-	-	-	-
	- airframe aft	4	4	4	-	-	-	8	8
	horizontal tail type:	-	-	-	-	-	-	-	-
	- with elevator	2	2	2	-	-	-	-	-
	- V-type	-	-	-	-	-	-	2	5
	- tailless	-	-	-	10	6	6	-	-
	vertical tail:	-	-	-	-	-	-	-	-
	- airframe aft	-2	-2	-1	-	-	-	8	8
	- on wing	-	-	-	-	5	5	-	-
	vertical tail type:	-	-	-	-	-	-	-	-
	- fixed	-	-	-	8	-	-	-	-
	- with rudder/ruddervator	3	4	3	-	3	3	-	-
7.	Landing gear:	-	-	-	-	-	-	-	-
	- changeable pads	-4	-	-4	7	5	-	-2	-
	- chute system	-	0	-	-	-	0	-	0
8.	Airframe:	-	-	-	-	-	-	-	-
	- long airframe	-2	-2	-	-	-	-	-2	-2
	- short airframe	-	-	-2	10	9	10	-	-
9.	Actuators:	-	-	-	-	-	-	-	-
	- electric	-7	-6	-8	9	8	8	-1	-1
10.	Materials:	-	-	-	-	-	-	-	-
	- composites	-2	-2	-2	2	2	2	-2	-2
	- wood/plywood	-3	-3	-3	3	3	3	0	0
	- foam	-3	-2	-2	4	6	6	0	0

The results of the calculation are shown in Table 2.2.

Table 2.2.

Objective parameter result table

No.	Technical performance measures	Weighted value, % ( $P_x$ )	A	B	C	D	E	F	G	H
1.	Cost ( $CI$ )	9	-2,79	-1,71	-1,08	4,14	2,43	1,62	0,09	-0,54
2.	Construction time ( $TI$ )	4	0,36	0,24	0,52	0,68	0,52	0,36	0,6	0,24
3.	Air vehicle weight ( $WI$ )	7	-2,1	-2,03	-1,33	2,52	1,96	0,7	-1,05	-1,75
$DI_{min}$ :		<b>20</b>	<b>-4,5</b>	<b>-3,5</b>	<b>-1,9</b>	<b>7,3</b>	<b>4,9</b>	<b>2,7</b>	<b>-0,4</b>	<b>-2,1</b>
4.	Performance ( $PI$ )	15	0,3	1,35	0,3	5,7	6	5,1	0,75	2,4
5.	Flying quality ( $FI$ )	20	4,2	4,2	3,8	-2,4	0	0	3	3
6.	Appearance ( $BI$ )	1	-0,11	-0,11	-0,11	0,1	0,06	0,07	0,05	0,07
7.	Maintenance ( $MI$ )	14	-0,32	-0,38	-0,41	0,49	0,18	0,17	-0,07	-0,06
8.	Manufacturability ( $RI$ )	10	0	-0,3	-0,3	1,2	0,4	0,4	0	-0,3
9.	Disposal ( $DI$ )	2	0,1	0,12	-0,14	0,24	0,26	0,26	0,04	0,06
10.	Stealth ( $SI$ )	18	-2,16	-1,98	-1,98	1,62	-0,54	-0,36	-0,9	-0,9
$DI_{max}$ :		<b>80</b>	<b>2,0</b>	<b>2,9</b>	<b>1,2</b>	<b>6,9</b>	<b>6,4</b>	<b>5,6</b>	<b>2,9</b>	<b>4,3</b>

As mentioned above, the construction priority  $P_{max}$  is greater than  $P_{min}$ , so the optimum configuration is the one that has obtained the highest value of the construction index  $DI_{max}$ . The results show that aircraft configuration D has the most optimal configuration [26]–[28].

## 2.2. Chapter summary and conclusions

In this chapter calculations for the first phase of the UAS conceptual design were completed, that is, the conceptual phase in which the most optimal type of the air vehicle was chosen by the multidisciplinary optimization method that meets the design requirements. During the calculation process, the numerical, measurable manner was successfully applied to determine the most optimal characteristics of the aircraft type that meet the design requirements.

### 3. PRIMARY CONSTRUCTION PHASE

According to Table 3.1, the tasks of the initial design phase are to determine the maximum take-off weight (*MTOW*), engine power and wing reference area of the aircraft. The initial load diagram of the UAV aircraft will be constructed based on the parameters obtained during this design phase.

Table 3.1

A summary of four major aircraft design phases [14; 20]

No.	Construction phase	Construction activity
1.	Conceptual design	Aircraft configuration selection.
2.	Preliminary design	Determine: (i) aircraft maximum take-off weight; (ii) engine power; (iii) wing reference area.
3.	Detail design	Part I: Design dominant components such as wing, fuselage, tail, and propulsion system, landing gear (nonmechanical); Part II: Design secondary components such as landing gear (mechanical), engine, structural design, avionic system, electric system.
4.	Tests and evaluation	Aircraft aerodynamic testing: wind tunnel test using aircraft model; Aircraft flight dynamic testing: flight test using a prototype; Aircraft structural testing using; Propulsion system testing using.

#### 3.1. Maximum take-off weight (MTOW) of aircraft

This chapter specifies the maximum initial UAV weight.

Maximum take-off weight of the UAV:

$$W_{\text{MTOW}} = (M_{\text{PL}} + M_{\text{A}} + M_{\text{AK}} + M_{\text{E}}) \times g = 86.328 \text{ N} \quad (3.1)$$

The refined calculation of UAV weights based on potentially usable elements as well as on the originally determined take-off weight using the graphical method (*matching plot method*), the reference area and engine power of the UAV wing are determined.

After the initial assessment, the maximum take-off weight of the UAS shall be:

$$W_{\text{MTOW}} = (M_{\text{PL}} + M_{\text{A}} + M_{\text{AK}} + M_{\text{E}}) \times g = 78.61 \text{ N} \quad (3.2)$$

After the resulting take-off weight, the wing reference area and the required electric motor power are determined using the graphical method.

Taking into account the calculation algorithm, the following parameters are calculated: wing loading parameter  $(W/S)_{V_s}$ , power loading at maximum speed  $(W/P_{SL})_{V_{max}}$ , power loading parameter  $(W/P)_{S_{TO}}$ , rate of climb parameter  $(W/P)_{ROC}$ , maximum cruising flight parameter  $(W/P_{SL})_C$  and absolute ceiling parameter  $(W/P_{SL})_{AC}$ . Then, the resulting chart is composed.

### Resulting chart

**Step 1.** Outline the results of all equations in the same graph. The power loading  $(W/P)$  shall be marked on the horizontal axis and the wing loading  $(W/S)$  on the vertical axis. The graph represents the change in power loading depending on the change in wing loading.

Using in previous step calculated parameters, a compliance chart in the MATLAB environment is constructed. The MATLAB code for the compliance chart is shown in Annex 2.

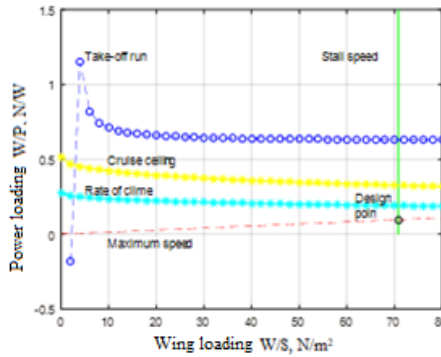


Fig. 3.1. Compliance chart with design point.

Determine the design point (optimum size). The design point in the graph is only one, which shows the smallest engine in terms of power.

As all parameters are met only by the area below the lowest graph, the design point is then searched below or at the line of the  $V_{max}$  graph, that is, the point forming the line of the maximum speed ( $V_{max}$ ) and the stall speed ( $V_s$ ) graph at the intersection.

**Step 2.** Two values are obtained from the structural point: the corresponding wing loading  $(W/S)_d$  and the power loading  $(W/P)_d$ .

$$(W/P)_d = 0.0963; \quad (3.3)$$

$$(W/S)_d = 70.805. \quad (3.4)$$

**Step 3.** Calculate the wing area and engine power from these two acquired values (the maximum take-off weight  $W_{TO}$  of the aircraft has already been determined above), using the following equations.

The design wing area and engine power shall be calculated as follows:

$$S = W_{TO}/(W/S)_d = 78.61/70.805 = 1.1102 \text{ m}^2. \quad (3.5)$$

$$P = W_{TO}/(W/P)_d = 78.61/0.0963 = 816.303 \text{ W} \sim 0.82 \text{ kW}. \quad (3.6)$$

**Step 4.** As mentioned in the calculation section of the maximum speed, when the engine power is obtained from the design results of the compliance chart, the zero lift-drag coefficient is recalculated by Eq. (3.7):

$$C_{D_0} = \frac{2 \times \frac{P_{SL_{max}} \times \eta_P}{V_{max}} - \frac{4 \times K \times W^2}{\rho \times \sigma \times V_{max}^2 \times S}}{\rho_{SL} \times V_{max}^2 \times S} = 0.024507 \quad (3.7)$$

Zero lift-drag coefficient,  $C_{D_0} = 0.024507$ , is obtained, which corresponds in practice to that originally calculated.

After optimization, the required electric motor power is also lower ( $\sim 817$  W) than originally assumed (900 W) [14]–[17], [31].

### 3.2. Construction of the UAS aircraft flight envelope

In this section a UAV flight envelope chart is calculated.

The flight envelope diagram was constructed in the MATLAB program, the code of which is shown in Annex 3.

According to the certification specification of the very light aircraft of the European Aviation Safety Agency (EASA) CS-VLA 333, wind gusts load varies linearly between speeds  $V_C$  and  $V_d$  [14]–[17], [30], [31].

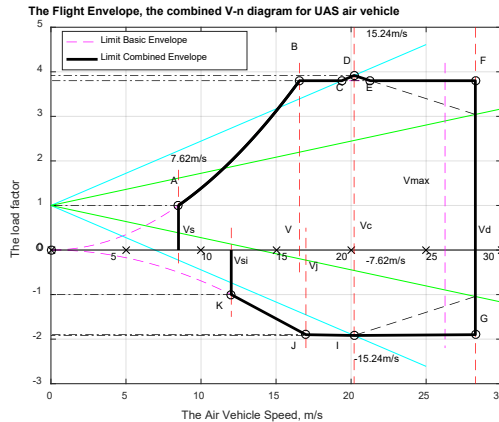


Fig. 3.2. UAV flight envelope.

### 3.3. Chapter summary and conclusions

This chapter examined the basic elements that are mounted on the unmanned aerial vehicle in order to be able to perform calculations and determine its main parameters (wing reference area and electric motor power) necessary to perform calculations in subsequent detailed construction phase. The process allowed to get to know the various electronics elements of the UAS vehicle, also the avionics, which were useful for selecting the most appropriate element in the further detailed calculation phase. A calculation program, based on the MATLAB, was

developed, to determine the main construction parameters, allowing it to be easily applied for construction calculations and also to recalculate parameters when necessary. The UAV load chart was also constructed. A program based on the MATLAB was also developed in this case to calculate the flight envelope chart, which makes it easy to recalculate when needed.

## 4. DETAIL CONSTRUCTION PHASE

According to Table 3.1, the tasks of the detailed engineering phases are the construction of dominant components – wing, tail, engine system, landing system (non-mechanical) – and the construction of secondary components – landing system (mechanical), motor, housing, avionics, electrical system, and actuators.

### 4.1. Wing construction

In this section, the airfoil for the construction of the wing was initially selected following the system engineering approach, in ten steps, calculating the basic parameters to meet the UAV design requirements.

Assessing all parameters (angle of fall –  $\alpha_s$ ,  $(C_l/C_d)_{\max}$  ratio, etc.) affecting the achievement of the design requirements, it is decided to make the wing of two airfoil profiles: Eppler e 186 and Wartman fx66h80 [14]–[17], [31], [37].

The design parameters for the wing at the assumed sweep angle of  $30^\circ$  for a 50 % chord line length are then calculated. The specified parameters are wing stroke  $b = 2.9802$  m, wing mean chord length  $\bar{C} = 0.372525$  m, wing root chord length  $C_r = 0.4562$  m, wing tip chord length  $C_t = 0.2737$  m, wing effective span  $b_{\text{eff}} = 2.5809$  m, wing effective aspect ratio  $AR_{\text{eff}} = 5.99 \sim 6$ , wing leading edge sweep angle  $\Lambda_{LE} = 32.95^\circ$ , wing quarter-chord sweep angle  $\Lambda_{C/4} = 31.50^\circ$ , wing trailing edge sweep angle  $\Lambda_{TE} = 21.83^\circ$  and location of the aerodynamic centre coordinate on x-axis  $X_N = 0.4766$  m [14]–[17], [31].

### 4.2. Winglet design parameters calculation

The following winglet parameters were determined:

- the sweep angle;
- the cant angle;
- the twist angle;
- the toe angle.

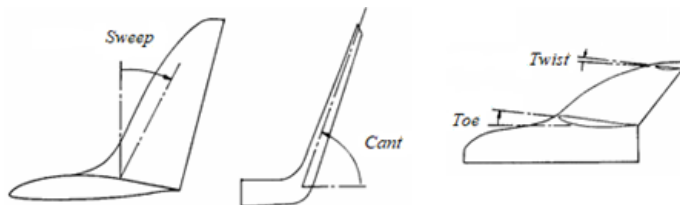


Fig. 4.1. Winglet design parameters [31].

As a result, the best performance is with the following winglet parameters:

- the sweep angle –  $70^\circ$ ;
- the cant angle –  $75^\circ$ ;

- the twist angle –  $0^\circ$ ;
- the toe angle –  $-0.2^\circ$ ;
- height: 140 mm.

The wing model in the *CFD OpenVSP* program with the above parameters is shown in Annex 4, Fig. 6.

Wing parameters were also determined in the *Computational Fluid Dynamics* program *SolidWorks Flow Simulation*. The first step was to prepare the computational domain and mesh, which is done automatically in the program. The prepared computational domain and mesh are shown in Annex 5, Fig. 1.

Based on the obtained computational results, the charts of  $C_L$ ,  $C_D$  and the  $C_L/C_D$  ratio variation depending on the angle of attack  $\alpha$  were constructed. Figure 2 in Annex 5 shows the  $C_L$  vs  $\alpha$  variation graph, showing the incremental increase of the lift factor  $C_L$  in the range of the angle of attack from  $0^\circ$  to  $8^\circ$ ; further as the angle of attack increases, the lift factor  $C_L$  decreases.

From the lift factor  $C_L$  to the angle of attack  $\alpha$  graph in Fig. 2 of Annex 5, can be seen that the value of the maximum lift factor  $C_L$  is at the angle of attack  $\alpha$  value of  $8^\circ$ . Taking into account the angle of wing setting  $\alpha_{set}$ , which is  $4.6^\circ$ , the total angle of attack for the stalling flight is  $12.6^\circ$ , which is greater than initially determined in the selection process of the wing airfoil section.

### **4.3. The wing parameter optimization calculation**

This section calculates the optimization of wing parameters resulting in changes to the wing structure.

In this case, the algorithm remained the same and will not be repeated, but it shows the results in Table 4.1. The calculation was made in the MATLAB program, the code of which can be viewed in Annex 14.

Table 4.1

## Wing Parameters after Optimization

No.	Name	Parameter designation	Size	Unit of measure
1	Wing reference area	$S_{ref}$	1.1102	m <sup>2</sup>
2	Aspect ratio	$AR_{eff}$	5	-
3	Tapper	$\Lambda$	0.6	-
4	Wingspan	$b_{eff}$	2.356	m
5	Mean aerodynamic chord	$MAC$	0.471	m
6	Wing root chord	$C_r$	0.577	m
7	Wing tip horde	$C_t$	0.346	m
8	Wing leading edge sweep angle	$\Lambda_{LE}$	30.88	degrees
9	Wing quarter-chord sweep angle	$\Lambda_{C/4}$	28.77	degrees
10	Wing trailing edge sweep angle	$\Lambda_{TE}$	14.31	degrees
11	Mean aerodynamic chord distance on y-axis	$Y$	0.540	m
12	Distance of the neutral point on x-axis from the top of the wing	$X_n$	0.441	m
Parameters obtained for wing without vinglets in <i>CFD</i>				
13	Lift-drag ratio	$L/D$	21.78	-
14	Angle of attack at maximum $L/D$ ratio	$\alpha$	3.2	-
15	Wave drag	$C_{D0\_w}$	0.0405	-
16	Parasitic drag	$C_{D0}$	0.00635	-
Parameters obtained for wing with vinglets in <i>CFD</i>				
17	Lift-drag ratio	$L/D$	22.62	-
18	Angle of attack at maximum $L/D$ ratio	$\alpha$	1.1 –3.2	-
19	Wave drag	$C_{D0\_w}$	0.0267	-
20	Parasitic drag	$C_{D0}$	0.00647	-

#### 4.4. Selection and calculation of landing system

##### Overview of existing landing systems

A study of the existing systems has shown that, in the UAV category under construction, aircraft landings are made in the following ways:

- deep stall landing;
- landing with a parachute;
- catching in net mechanism;
- catching with a hook mechanism.

The first two ones of the above are more used when the aircraft is launched manually. These systems require additional equipment, and the aircraft itself must have a sufficiently robust structure that increases the weight of the aircraft itself and the system as a whole.

### ***Landing procedure***

One of the parameters for the aircraft performance assessment is the length of its landing path. Preferably, the landing performance of the aircraft is the shortest possible landing path. The landing path is measured starting from an imaginary obstacle, over 15 m height, to full stop. The aircraft speed  $V_L$  at the start of the landing procedure is calculated from the stall speed  $V_S$  or  $V_L = 1.3 \times V_S$ , in this case  $V_L = 1.3 \times 8.5 = 11.05$  m/s. The UAV landing process is completed in three phases: (1) approach, (2) glideslope and dynamic stall, and (3) brake [31].

According to the calculations performed, the total length of the required landing path with the glideslope and ground run shall be 113.7 m, assuming that the initiation of the landing procedure is commenced at an altitude of 18 m. The distance is calculated together with the  $L_{\text{Recovery}}$  value and shows the distance the UAV slips along the ground surface after contact to full rest [48]–[50].

In order to reduce the horizontal velocity component that is especially high in shallow landing glideslopes, an additional *dynamic stall* process shall be incorporated into the landing process. This is in the final stage of the landing flight path, when the UAV is already practically close to the ground contact (height marked with  $\Delta h_{\text{Recovery}}$ ), it is introduced into a high angle of attack position above the aircraft's stall angle, thus rapidly increasing the lifting force temporarily and reducing the horizontal speed. This corresponds to the landing process where the height at which the UAV can be entered in the dynamic stall state is 1.5 m [20].

### **Alternative landing method**

The usage of the UAV is growing, but it is an expensive technology, therefore its main course of expansion is in the military and interior structures. In these areas, the UAV may be used in particularly burdensome circumstances, such as those where there is a very small open area, or in certain situations when a quick landing may be required, which can be done in the way offered in the Thesis. In such circumstances, it is proposed to use an alternative way of landing the UAV using extreme flight conditions, i.e., at the required UAV landing position, it is introduced into the stall followed by the spin. Approaching the ground in the spinning flight condition, at an approximate altitude of 3 m above the ground surface, the UAV flight condition is stabilized with a continuation of the circular landing flight path trajectory until the moment of touchdown.

If the flight path is continued along a circular/orbital flight path after recovery from the spin, then the area required for the UAV landing will be significantly smaller, up to 10 m in diameter, which corresponds to the requirements to land the UAV on a restricted open area (where there are no obstacles to flight operations, that is, no trees, shrubs or any structures and constructions).

The following was of the last phase of the landing flight may be considered :

- in a linear gliding flight path with a shallow flight path angle  $\gamma = 3^\circ$ ;
- an orbital/circular flight path with a radius equal to approximately half the wing length, i.e.,  $R = b/2$ ;

- the possibility to complete the final landing phase with the deep stall.

In the first proposed landing option, the final landing phase requires a clear path of 28–37 m, which does not meet the design requirements for the UAV landing on a restricted open area. This distance can be reduced by initiating exit from the spinning flight as close as possible to the ground surface and increasing the angle of the landing flight path. In this case, a very sensitive and accurate sensor is required, the operation of which should be coordinated with the elevator handling time, for which additional research is necessary.

The second proposed final landing phase option fully satisfies the design requirements. It would be possible to land the UAV on a free area not exceeding 8 m in diameter. Again, additional research is required to determine the optimum flight path orbit radius.

The third proposed final landing phase option could also satisfy the design requirements, but at the same time it potentially increases the complexity of the UAV itself. This option would require further research. In this case, it would also be necessary to stabilize the UAV flight from spin as close as possible to the ground surface.

The approach of the aircraft to the landing point is performed with the on-board navigation equipment – GPS, INS and AHRS and autopilot settings. The coordinates of the landing location are set in the autopilot, and the preprogrammed landing system is selected from the abovementioned types. The aircraft in position of set landing coordinates enters into a controlled stall followed by the spin. Approaching the ground surface, after an initial assessment at ~ 3 m altitude, flight stabilization is activated, i.e., with elevons, the aircraft is stabilized close to the horizontal flight path but continues the circular/orbital flight path until the landing touchdown moment [8]–[11].

The aircraft altitude, during its landing process (*SSLC – stall–spin landing code*), can be controlled with *LiDAR* laser sensor the possible models of which could be *STMicroelectronics VL53L1X* or *Benewake TFmini*.

#### 4.5. Innovative take-off system selection and calculation

To facilitate the overall weight of the UAV system, it is offered in the design to use for the UAV launch the hand launch system, without a catapult. When launching a UAV by hand, the operator shall itself develop sufficient acceleration to produce the required lifting capacity, which may be problematic at the design weight.

In the light of the above, it is proposed to take off the aircraft with an operator-generated circular/orbital run path. The moment of launch of the aircraft in flight may, as the case may be, continue in a straight direction, i.e., tangential to the orbit or with an orbital motion progressively increasing radius until the required flight altitude is reached at least above the nearest obstacle height [14], [31].

Gravity by its components in the body coordinate system shall be expressed as follows:

$$F_g = \begin{pmatrix} -m \times g \times \sin \theta \\ m \times g \times \cos \theta \times \sin \phi \\ m \times g \times \cos \theta \times \cos \phi \end{pmatrix}. \quad (4.1)$$

The rate of flight relative to the ground in the inertial coordinate system, and assuming  $V_g = V_a$ , shall be expressed as follows:

$$V_g^i = V_g \times \begin{pmatrix} \cos \psi \times \cos \gamma \\ \sin \psi \times \cos \gamma \\ -\sin \gamma \end{pmatrix}. \quad (4.2)$$

As the minimum speed to be provided by the operator in orbital motion for  $F_{\text{net}} \geq F_g$  is determined, and taking into account Newton's second law, the minimum orbital flight speed can be determined by the Eqs. (4.3):

$$V_g^i = \sqrt{\frac{F_{g-\text{net}} \times R}{m}} \times \begin{pmatrix} \cos \psi \times \cos \gamma \\ \sin \psi \times \cos \gamma \\ -\sin \gamma \end{pmatrix}. \quad (4.3)$$

According to the calculation, for the UAV in steady circular or orbital motion, the required speed shall be 3.8 m/s, provided that the orbit radius is 1.5 m. The calculation was made in the MATLAB program, the code of which is shown in Annex 5.

The aircraft's orbital flight path is expressed by the following equation [37]:

$$P_{\text{orbit}}(c, \rho, \lambda) = \{r \in R^3 : r = c + \lambda \times \rho \times (\cos \varphi, \sin \varphi, 0)^T, \varphi \in [0.2 \times \pi]\}. \quad (4.4)$$

The orbit trajectory is characterized by its center  $C \in R^3$ , radius  $\rho \in R$  and direction  $\lambda \in \{-1, 1\}$ , where  $\lambda = 1$  is the direction of orbit clockwise and  $\lambda = -1$  is the direction of orbit anticlockwise. It is assumed that the center of orbit is determined in the inertial coordinate system with  $C = (C_n, C_e, C_d)$ , where  $C_d$  expresses the desired height of orbit, and to maintain altitude, it is assumed that  $h_C = -C_d$ . When flying the UAV at constant altitudes, its coordinates in the polar coordinate system can be derived from differential equations describing the movement of the aircraft in the northern and eastern directions, i.e.:

$$\begin{pmatrix} p_n \\ p_e \end{pmatrix} = \begin{pmatrix} V_g \times \cos \chi \\ V_g \times \sin \chi \end{pmatrix}, \quad (4.5)$$

carried out with the phase angle  $\varphi$  in such a way that the motion equations represent the movement of the aircraft in a normal and tangential direction towards the orbit as follows:

$$\begin{pmatrix} \dot{d} \\ d\dot{\varphi} \end{pmatrix} = \begin{pmatrix} V_g \times \cos(\chi - \varphi) \\ V_g \times \sin(\chi - \varphi) \end{pmatrix}. \quad (4.6)$$

It was assumed that the aircraft had to rise to a height of 30 m, where it could continue flying (*loitering*) motion and wait for the entry of a subsequent task, flight route.

As shown in Fig. 4.2,  $d$  represents the radial distance from the desired orbit center location to the aircraft, and  $\varphi$  is the phase angle of the relative location.

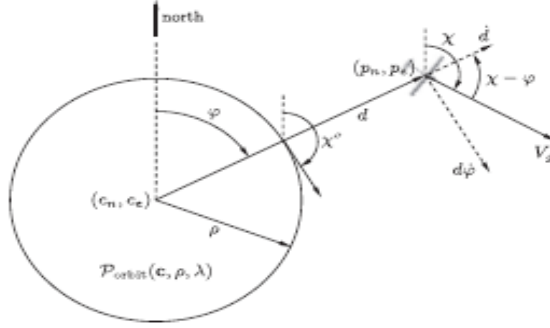


Fig. 4.2. Parameters of the orbital flight [41].

The dynamics of the UAV in the polar coordinate system can then be characterized by the following equations:

$$\dot{d} = V_g \times \cos(\chi - \varphi), \quad (4.7)$$

$$\dot{\varphi} = \frac{V_g}{d} \times \sin(\chi - \varphi), \quad (4.8)$$

By treating the orbital trajectory referred to the situation at issue in the current work, that is for a take-off event, Eq. (4.6) should be rewritten as follows:

$$\begin{pmatrix} \dot{d} \\ \dot{\varphi} \\ \dot{h} \end{pmatrix} = \begin{pmatrix} V_g \times \cos(\chi - \varphi) \\ V_g \times \sin(\chi - \varphi) \\ V_g \times -\sin(\chi - \gamma) \end{pmatrix}. \quad (4.9)$$

A graphical representation of the trajectories is shown in Figs. 4.3 and 4.4 [19], [40], [41].

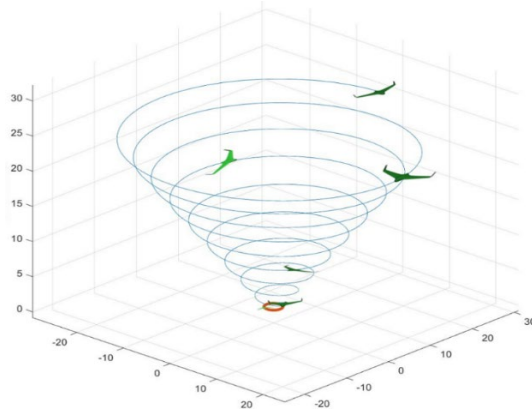


Fig. 4.3. The trajectory of the orbital climb after the orbital run.

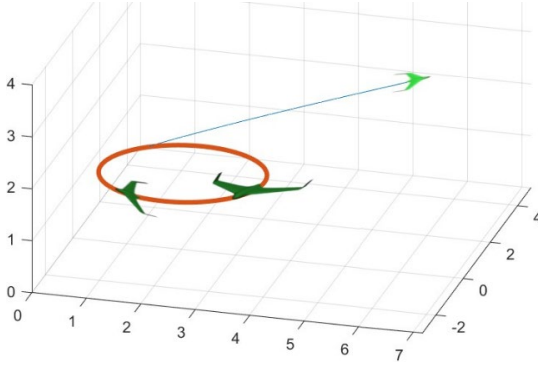


Fig. 4.4. Linear climb path after the orbital run.

The calculation was made in the MATLAB program, the code of which is shown in Annex 5. The use of the orbital take-off system is shown in Annex 7.

## 4.6. Engine system selection and calculation

### Calculation and selection of propeller

The propeller of the aircraft, on a steady cruising flight at  $V_C$  and the propeller efficiency  $\eta_P$ , will develop the thrust, which is the engine power function, as follows:

$$T = \frac{P \times \eta_P}{V_C} = \frac{612.22725 \times 0.8}{26} = 18.8378 \text{ N}, \quad (4.10)$$

where  $P$  is the engine power.

The propeller will develop the lifting capacity in the direction of flight as follows:

$$L_P = \frac{1}{2} \times \rho \times V_{av}^2 \times S_P \times C_{LP}, \quad (4.11)$$

where

$\rho$  – the air density at the altitude of the cruising flight;

$S_P$  – floating area of the propeller;

$C_{LP}$  – the load factor of the propeller;

$V_{av}$  – the average airspeed at the propeller, which can be assumed to be 70 % of the propeller tip  $V_{tipcruise}$  speed.

It should also be noted that the propeller-developed lifting capacity ( $L_P$ ) is equal to the engine thrust ( $T$ ), so the following can be written:

$$L_P = T \Rightarrow \frac{1}{2} \times \rho \times V_{av}^2 \times S_P \times C_{LP} = \frac{P \times \eta_P}{V_C} = 18.8378 \text{ N}. \quad (4.12)$$

The typical relative aspect ratio of the propellers  $AR_P$ , values are between 7 and 15 and the lifting coefficient  $C_{LP}$  is between 0.2 and 0.4, which are accepted between 11 and 0.3, respectively. From the previous calculations, the cruising flight velocity  $V_C$  is between  $20.20 \div 26$  m/s. It should also be noted that the cruising flight is calculated at 75–80 % engine power, then:

$$D_{P1} = K_{np} \times \sqrt{\frac{2 \times P \times \eta_P \times AR_P}{\rho \times V_{av}^2 \times C_{LP} \times V_C}} = 0.3153 \text{ m} \quad (4.13)$$

and

$$D_{P2} = K_{np} \times \sqrt{\frac{2 \times P \times \eta_p \times AR_p}{\rho \times V_{av}^2 \times C_{Lp} \times V_C}} = 0.2779 \text{ m} \quad (4.14)$$

where

$K_{np}$  is the correction factor for the propeller, a two-wing propeller, that is 1, but if more wings are required, then it is  $< 1$ .

So, the required propeller diameter is between  $\sim 280 \div 320$  mm, or because the size of commercially offered propellers is usually marked in inches, then  $\sim 11''\text{--}13''$  assuming an average value of  $D_P = 12''$ , which will be corrected if necessary in a further construction process.

Respectively, propeller rotation speed

$$V_{tipcruise} = \sqrt{V_{tipstatic}^2 + V_C^2} = \sqrt{168^2 + 20.20^2} = 169.21 \frac{\text{m}}{\text{s}} \quad (4.15)$$

or

$$V_{tipcruise} = \sqrt{V_{tipstatic}^2 + V_C^2} = \sqrt{168^2 + 26^2} = 170.00 \frac{\text{m}}{\text{s}}.$$

Assuming that it will also be necessary to fly at maximum speed, then

$$V_{tipcruise} = \sqrt{V_{tipstatic}^2 + V_C^2} = \sqrt{246^2 + 33.8^2} = 248.31 \frac{\text{m}}{\text{s}} \quad (4.16)$$

and

$$V_{tipstatic} = \frac{D_P}{2} \times \omega \Rightarrow \omega = \frac{2 \times V_{tipstatic}}{D_P} = \frac{2 \times 250}{0.3} = 1\,666.66 \frac{\text{rad}}{\text{s}}, \quad (4.17)$$

then

$$n = \frac{60 \times \omega}{2 \times \pi} = \frac{60 \times 1666.66}{2 \times 3.14} = 15\,923.50 \text{ rpm} \sim 15\,924 \text{ rpm}. \quad (4.18)$$

The engine selection shall take into account that the maximum speed is 16,000 rpm/min [6], [23].

### Calculation and selection of electric motor

Following multidisciplinary optimization, the electric motor **B50-10S** of the manufacturer Hacker motor GmbH was selected. The parameters of the abovementioned engine will be taken into account in the subsequent calculations. Refer to Annex 6 [26]–[29], [52] for an optimization table for the choice of electric motor and data for the selected electric motor.

## 4.7. Battery selection

Following multidisciplinary optimization of the battery models, the battery **NCR20700B** of the manufacturer Miuta Electric company was selected. If an alternative solution is needed, the possibility of using two types of batteries in the system that reduce the total weight by 270 g will be considered, but it should be taken into account that a voltage booster unit will be required [26]–[29].

## 4.8. Selection of avionics components

### Autopilot selection

Following multidisciplinary optimization, five models were selected from available autopilot models, which obtained the highest score and had other desired technical parameters (A, E, F, G, K). Alternative models will also be selected in case construction objectives are not initially met. View the autopilot selection optimization table and selected autopilot data in Annex 8 [26]–[29], [53], [54].

### Choosing GPS/INS/AHRS

Following multidisciplinary optimization of available *GPS/INS/AHRS* models, the GPS manufacturer's NovAtel model *OEM7720* was selected with manufacturer's Trimble antenna *AV16* and manufacturer's VectorNav inertial navigation device *VN-300*, which is technically compatible with the selected autopilots and gained a relatively high rating and will be integrated into the common system with autopilot. The highest GPS position was obtained by the manufacturer's Trimble model *BD940* and, in the GPS/INS manufacturers' Trimble and *LORD* sensing positions, *APX-18 UAV* and *3DM-GQ4-45* respectively, which will be considered if construction targets are not met and a compromise solution is required. See GPS/INS/AHRS optimizing table and data in Annex 8 [26]–[29], [53], [54].

### Selecting a data terminal

Following multidisciplinary optimization of available data terminal models, the manufacturer's CloudCap Technology data terminal model, *Piccolo Nano*, was selected, which obtained the highest rating and will be integrated into a common system with autopilot. See Annex 8 for an optimization table and data for the selection of the data terminal [26]–[29], [53], [54].

### Selecting a transponder

Following multidisciplinary optimization of available transponder models, the manufacturer Aerobits model *TIM-MCI* was selected, which obtained the highest rating and will be integrated into the common system with autopilot. See the optimizing table and data in Annex 9 [26]–[29], [53], [54].

### Construction of an avionics component module

The avionics module will consist of the following components, listed in Table 4.2, according to preliminary calculations and multidisciplinary optimization.

Table 4.2

List of Components of the UAV Avionics Module

No.	Component Model	Manufacturer	Function	Notes
1	Easypilot 3.0	Skyview	Autopilot	With integrated data terminal, GPS, INS (Ima, AHRS)
2	Piccolo Nano	Cloudcap Technology	GPS	-
3	AV16	Trimble	GPS antenna	It is not part of the module itself but must be mounted on it from the outside
4	TIM-MC1	Aerobit	Defendant	-

#### 4.9. Aircraft body construction

Based on the dimensions of the modules developed, the aircraft body in the *CAD* environment is constructed. The full body *CAD* model will be tested for performance parameters in the *CFD* program.

The *CAD* drawing of the aircraft model *CFD* program is shown in Fig. 4.5.

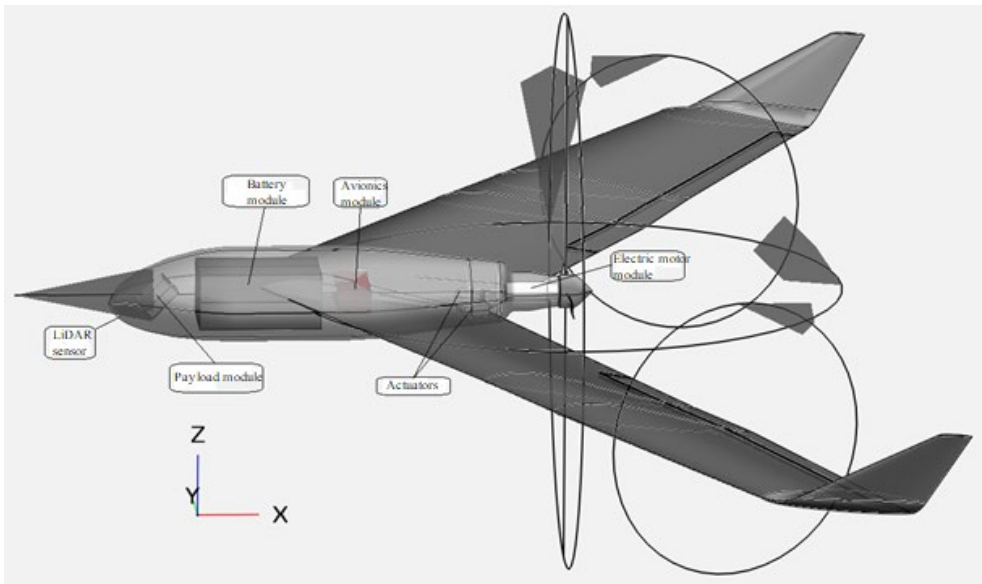


Fig. 4.5. The UAV projection in the *CFD* program.

#### 4.10. Selection of ground control station

The comparison of parameters was subjected to multidisciplinary optimization for available *GCS* models. See the *GCS* optimization table and data in Annex 10 [26]–[29].

### 4.11. Design and selection of payload element

This section calculates the value of the payload element sensors using the general image quality equation (GIQE) and makes their initial selection [55]–[57].

GIQE has seen several amendments. Version 4 is currently in force in the following form:

$$NIIRS = 10.251 - a \times \lg GSD_{GM} + b \times \lg RER_{GM} - 0.656 \times H_{GM} - 0.334 \times \left(\frac{G}{SNR}\right), \quad (4.19)$$

where

$GSD_{GM}$  – the geometric mean (GM) of the ground sampled distance (GSD) in inches;

$RER_{GM}$  – the geometric mean (GM) of the normalized relative edge response (RER);

$H_{GM}$  – the geometric mean height owing to edge overshoot resulting from modulation transfer function compensation (MTFC);

$G$  – intrusion of interference from MTFC;

$SNR$  – signal-to-noise ratio (SNR).

Sizes  $GSD_{GM}$  and  $RER_{GM}$  invest up to 92 % in the value of  $NIIRS$ . Others – only 8%.

The values of parameters  $a$  and  $b$  are as follows:

$$a = \begin{cases} 3.32, & \text{if } RER_{GM} \geq 0.9 \\ 3.16, & \text{if } RER_{GM} < 0.9; \end{cases}$$

$$b = \begin{cases} 1.559, & \text{if } RER_{GM} \geq 0.9 \\ 2.817, & \text{if } RER_{GM} < 0.9. \end{cases}$$

In summary, if the  $NIIR$  level is known before the task is completed, the sensor planning model is based on  $NIIRS$  and GIQE, as illustrated in Fig.4.6.

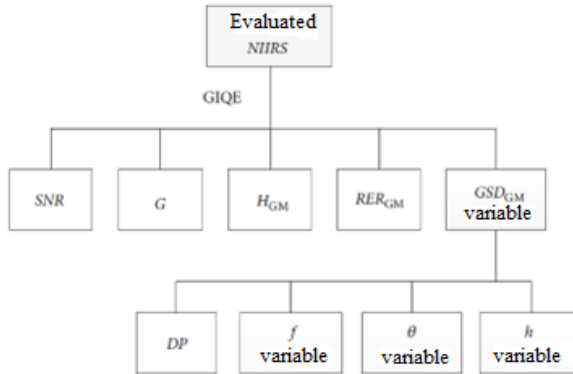


Fig.4.6. Sensor planning model based on  $NIIRS$  and  $GIQE$  [50].

The  $NIIR$  calculation was made in the MATLAB program, the code is shown in Annex 12.

According to the  $NIIR$  image interpretation scale in Annex 11, it is preferable that  $EO/IR$  sensors provide image quality according to levels 7 to 9, with the UAV flying at unidentifiable altitudes, respectively, at a predetermined level of 350 m above the ground [55]–[57].

#### Sensor pixel distance

The pixel distance is calculated for a desired performance, assuming that:

- focal length  $f = 30\text{--}60 \text{ mm} = 0.03\text{--}0.06 \text{ m}$ ;

- pixel projection  $x = y = 15 \text{ mm} = 0.015 \text{ m}$ ;
- sensor distance to the vertical plane of the image  $r = h \times \sin\alpha = 350/\cos 30^\circ \sim 405 \text{ m}$ ;
- assumes the same number of pixels horizontally and vertically.

$$DP = \frac{x \times f}{r} = \frac{0.015 \times 0.06}{405} = 2.22 \times 10^{-6} \text{ m} = 2.22 \text{ }\mu\text{m}. \quad (4.20)$$

and

$$DP = \frac{x \times f}{r} = \frac{0.015 \times 0.03}{405} = 1.11 \times 10^{-6} \text{ m} = 1.11 \text{ }\mu\text{m}. \quad (4.21)$$

The projected area is determined by Eq. (6.58) as follows:

$$S_{11} = \frac{DP \times DP' \times r^2}{f^2} = \frac{2.22 \times 10^{-6} \times 2.22 \times 10^{-6} \times 405^2}{0.06^2} = 0.0002246 \text{ m}^2 = 224.6 \text{ mm}^2 \quad (4.22)$$

and

$$S_{12} = \frac{DP \times DP' \times r^2}{f^2} = \frac{1.11 \times 10^{-6} \times 1.11 \times 10^{-6} \times 405^2}{0.06^2} = 0.00005614 \text{ m}^2 = 56.14 \text{ mm}^2 \quad (4.23)$$

and

$$S_{21} = \frac{DP \times DP' \times r^2}{f^2} = \frac{2.22 \times 10^{-6} \times 2.22 \times 10^{-6} \times 405^2}{0.03^2} = 0.0008982 \text{ m}^2 = 898.2 \text{ mm}^2 \quad (4.24)$$

and

$$S_{22} = \frac{DP \times DP' \times r^2}{f^2} = \frac{1.11 \times 10^{-6} \times 1.11 \times 10^{-6} \times 405^2}{0.03^2} = 0.0002246 \text{ m}^2 = 224.6 \text{ mm}^2 \quad (4.25)$$

From the results of the calculation above, it can be seen that the most desired result is with a pixel distance  $DP = 1.11 \text{ }\mu\text{m}$  and a focal distance  $f = 0.06 \text{ m}$ . A sensor with a pixel distance  $DP = 1.11 \text{ }\mu\text{m}$  will also be able to provide the desired result in the case of a lower focus distance ( $f = 0.03 \text{ m}$ ) if it is considered that the pixel distance of the projected image should be  $\sim 1.5 \text{ cm}$ , which makes up the projected area  $S = 225 \text{ mm}^2$  ( $S_{22} = 224.6 \text{ mm}^2$ ).

The preferred parameters are the *FSM-ARI335* for *EO* sensor module of the Framos company and the *ARI337* for *IR* sensor module of the ON Semiconductor company. The technical data of those sensors can be consulted in Annex 12 [58].

## 4.12. Chapter summary and conclusions

In this chapter the calculations were completed for the main structural parameters of the UAS vehicle and also for the selection of other elements. The wing configuration was selected and its parameters calculated. An electric motor shall be selected to provide the requirements in the most optimal manner, as well as other electronic elements, in such a way as to satisfy the structural requirements set out in the most optimal manner. Two conceptually innovative solutions were found to fulfil the take-off and landing functions of the UAS vehicle so that it can be carried out on a restricted free area, as may be the case with the system for special military or internal affairs purposes. Application in a restricted area may also occur if the system is used for nature observation purposes, if the area of the observation is located in a wooden environment.

## 5. TESTING THE DEVELOPMENT OF AN UNMANNED AERIAL VEHICLE SYSTEM

Knowing the exact parameters of a drone system aircraft, optimization of its flight parameters may be performed in order to obtain the desired flight duration in accordance with the design requirements.

This chapter will determine the aircraft's optimal parameters for cruising flight, gliding flight, maximum range flight speed, maximum endurance flight speed and corresponding required power.

### 5.1. Optimization of the flight parameters of an unmanned aircraft

This section defines the optimal flight parameters for UAV.

#### Gliding flight performance

Table 5.1 shows the parameters of the UAV aircraft that will be used for calculations.

Table 5.1

Aircraft Parameters

Aircraft weight	$m = 7.8792 \text{ kg}$
Wing reference area	$S = 1.1102 \text{ m}^2$
Design flight altitudes	$H_1 = 350 \text{ m}$ $H_2 = 400 \text{ m}$
Air density at gliding altitude	$\rho = 1.184 \text{ kg/m}^3$
Gravity acceleration	$g = 9.8067 \text{ m/s}^2$
The wing leading edge sweep angle	$\Delta_{LE} = 32.95^\circ$
Wing aspect ratio	$AR = 5$

Based on the parameters obtained, the parameter check was performed in the *CFD OpenVSP* program. The initial test was performed on the performance of the gliding flight. Accordingly, the following parameters were calculated in the program: cruising flight maximum lift coefficient  $C_L = 0.51$  and ratio  $L/D = 27.50$ , as shown in the graph in Figs. 1 and 2 of Annex 20. From the graph  $L/D$  to  $\alpha$ , in Annex 20, Fig. 1, it can be read that the maximum ratio is the angle of uptake  $\alpha = 3.2^\circ$ , which is the gliding angle of attack and forms  $7.8^\circ$  and  $6.3^\circ$ , respectively, for the inner and outer sections of the wing. Figures 3 and 4 of Annex 20 show the vortices and pressure parameters for the gliding speed of  $14.12 \text{ m/s}$ . Figures 5 to 8 of Annex 20 show the performance of a wing with a winglet at the same gliding speed. From the parameters, it can be seen that at lower speeds the winglets work more efficiently, with vortices more than 3.5 times less ( $0.00123$ ) than without the winglets ( $-0.00447$ ), and the lift coefficient has increased by  $7.8 \%$ .

UAV parameters were also determined using the *Computational Fluid Dynamics ANSYS Fluent* program. At first, the *ANSYS ICEM* program was used to prepare a computational

domain and mesh where a finer and denser network was prepared near UAV for better capture of the flow in the boundary layer. The prepared computational domain and mesh are shown in Annex 21, Fig. 1.

Based on the computational results obtained, the graphs of variation of the  $C_L$ ,  $C_D$  and  $C_L/C_D$  ratio to the angle of attack  $\alpha$  were constructed. Figure 3 of Annex 21 shows a graph of variation of the  $C_L$  vs  $\alpha$ , showing a gradual increase in the lift factor  $C_L$  in the range of the angle of attack from  $0^\circ$  to  $5^\circ$  (to approximately  $6^\circ$ ), followed by a sharp decrease in the lift factor  $C_L$  as the uptake angle increases.

The verification in the *CFD* program provided confirmatory information on the data previously obtained during the wing construction process, when the cross-section profile of the wing was selected, where the angle of stall for the selected profiles is  $\sim 10^\circ$  (see Table 6.2). Taking into account the *CFD* test carried out, with a UAV at angle of attack of  $6^\circ$  and a wing setting angle, the stall angles obtained by the testing in *CFD* are  $9.1^\circ$  and  $10.6^\circ$  respectively. The flow rate (10 m/s) used for the *CFD* test is more consistent with the UAV gliding flight speed, which is slower than the cruising flight speed and uses the UAV maximum  $L/D$  ratio value. The values previously determined in MATLAB for the most optimum gliding flight for designed UAV are  $V_{bg} = 14.9$  m/s and  $(L/D)_{max} = 15.97$ , respectively. The maximum  $L/D$  ratio obtained during the *CFD* test is  $\sim 15.2$ .

A calculation of the UAS aircraft flight parameters was completed in the MATLAB program. The calculation code can be seen in Annex 18. The calculation resulted in the following parameters [59]:

$AoA = 0.72312^\circ$	$C_{l_{bg}} = 0.46035$	$CAS_{mr} = 15.64$ m/s
$(L/D)_{max} = 16.59$	$D_{bg} = 4.7265$ N	$P_{mr} = 74.188$ W
$CAS_{bg} = 15.83$ m/s	$L_{bg} = 78.4376$ N	$CAS_{mc} = 11.92$ m/s
$\gamma_{bg} = -3.45^\circ$	$CAS_{oc} = 21.84$ m/s	$P_{mc} = 67.0123$ W
$Cd_{bg} = 0.02774$	$D_{oc} = 5.4152$ N	$P_{oc} = 123.1382$ W

The final performance parameters are shown in the graphs below.

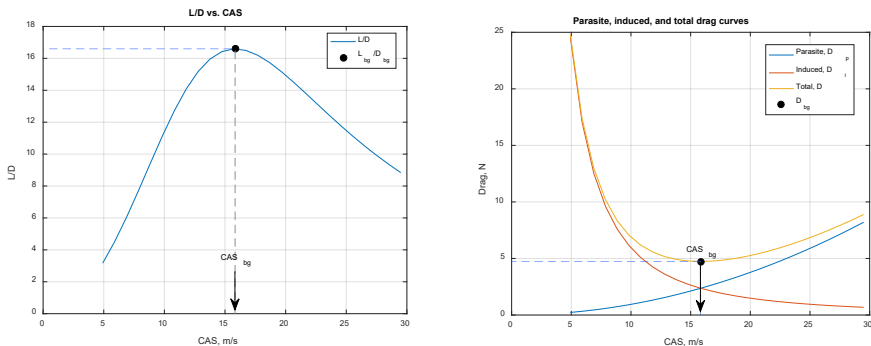


Fig. 5.1.  $L/D$  ratio depending on  $CAS$  schedule and resistance force curve and the corresponding flying speed ( $CAS_{BG} = 15.8295$  m/s).

According to the calculation, the optimum cruising flight speed has a power consumption of  $P_{oc} = 123.14$  W, which means the maximum flight duration according to the selected battery type is:

$$T = \frac{C}{P_{oc}} = \frac{849}{123.14} = 6.89 \text{ h.} \quad (5.1)$$

Taking into account the average consumption of 23 W of other consumers, which totals 146.14 W, then

$$T = \frac{C}{P} = \frac{849}{146.14} = 5.81 \text{ h.} \quad (5.2)$$

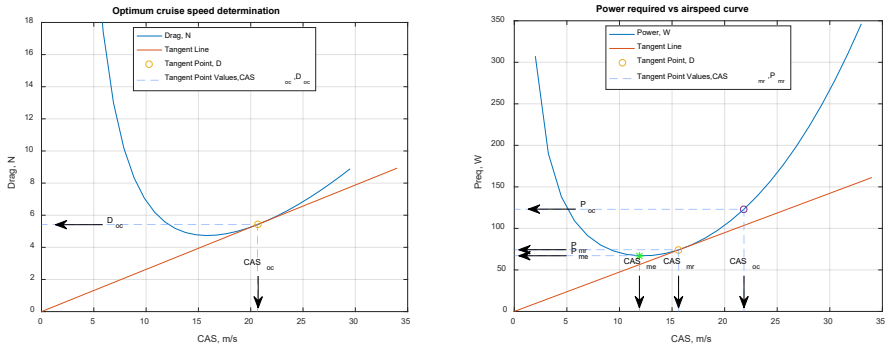


Fig. 5.2. The charts for determination of optimum cruising flight speed and maximum duration flight speed ( $CAS_{oc} = 21.84$  m/s,  $CAS_{mr} = 15.64$  m/s,  $CAS_{me} = 11.92$  m/s).

### Design goals

Based on the results obtained, a table of construction target results is drawn up.

Table 5.2

## Design Target Parameter Achievement

No.	Parameter	Claim	Result achieved	Notes
1	<i>MTOW</i>	up to 9 kg	7.8792 kg	Calculation weight
2	Engine type	Electric motor	√	-
3	Duration of flight	> 300 min	348.6 min	-
4	Useful flight height	> 300 m	350 m	EO/IR sensor adjustment according to calculations
5	Launch height	< 5 000 m	15,000 m	Autopilot maximum height
6	Operating distance	at least 50 km	√	Achievable at increased power up to 10 W
7	Payload	EO/IR camera	√	Individually customizable
8	Modular aircraft, portable in a rucksack in disassembled form	Assembly time: < 10 min (ready to run)	√	Designed to meet the requirements, modular
9	Launch system	Hand-operated	√	Designed to meet the requirements

## 5.2. Unmanned aerial vehicle system aircraft optimization

The aircraft's conceptual design phase has six most important parameters for optimization:

- T/W or P/W (defined engine size by ratio);
- W/S (defined wing size by ratio);
- the wing aspect ratio  $AR$ ;
- the wing taper ratio;
- the wing sweep angle;
- the wing airfoil  $t/c$ .

These six parameters determine the performance values of the aircraft such as engine power and wing area and the basic geometric shape of the wing. These parameters are also at the core of the optimization process during the design phase of the aircraft [27]–[29].

## 5.3. Chapter summary and conclusions

The calculations made in this chapter verified that the results obtained during the conceptual design process conform with the design requirements. The results showed that the design is in the right direction and that the results meet the design requirements.

## 6. UNMANNED AIRCRAFT EXPERIMENTAL MODEL

A commercially available flying wing model, shown in Annex 18, was used for the experimental trial. A comparison of the parameters of the experimental and conceptual unmanned flying wing models is shown in Table 6.1.

Table 6.1

Comparison of Conceptual and Experimental UAV Model Parameters

No.	Name	Parameter designation	Conceptual model	Experimental model	Unit of measure	Scale match, %
1	Aircraft weight	$m$	7.88	1.8	kg	1 : 4.4
2	Electric motor power	$P$	0.82	0.23	kW	1 : 3.6
3	Propeller diameter	$D_P$	30.5	20.5	cm	-
4	Propeller pitch	$P_P$	15.0	10.0	cm	-
5	Wing reference area	$S_{ref}$	1.1102	0.2911	m <sup>2</sup>	1 : 3.8
6	Wing aspect ratio	$AR_{eff}$	5.00	5.00	-	-
7	Tapper ratio	$\lambda$	0.60	0.60	-	-
8	Span	$b_{eff}$	2.356	1.206	m	1 : 1.95
9	Mean aerodynamic chord	$MAC$	0.471	0.241	m	1 : 1.95
10	Wing root chord	$C_r$	0.577	0.295	m	1 : 1.95
11	Wing tip chord	$C_t$	0.346	0.177	m	1 : 1.95
12	Wing leading edge sweep angle	$\Lambda_{LE}$	30.88	25.29	degrees	-
13	Wing quarter-chord sweep angle	$\Lambda_{C/4}$	28.77	22.96	degrees	-
14	Wing trailing edge sweep angle	$\Lambda_{TE}$	14.31	7.39	degrees	-
15	Mean aerodynamic chord distance on y-axis	$Y$	0.540	0.276	m	-
16	Neutral point distance on x-axis from the tip of the wing	$X_n$	0.441	0.191	m	-

For the calculation of the flight parameters of the experimental aircraft, the same equations as those used in Chapter 5 will be used.

### 6.1. Drone experimental model flight parameters

This section compares the parameters of the UAV experimental and conceptual model.

From practical flights, the maximum flight speed may be between 50 km/h and 70 km/h or 13.89 m/s and 19.4 m/s depending on the configuration chosen. Based on the results obtained, a comparison table for flight parameters for conceptual and experimental models is drawn up.

Table 6.2

Comparison of Results

No.	Conceptual model parameters	Experimental model parameters	Notes
1	$AOA = 0.72312^\circ$	$AOA = 0.6961^\circ$	-
2	$(L/D)_{\max} = 16.5937$	$(L/D)_{\max} = 15.9696$	-
3	$Cas_{bg} = 15.8295 \text{ m/s}$	$Cas_{bg} = 14.9322 \text{ m/s}$	Practical cruising flight speed: 13.89–19.4 m/s depending on configuration
4	$Cas_{oc} = 21.84 \text{ m/s}$	$Cas_{oc} = 19.6658 \text{ m/s}$	
5	$Cas_{mr} = 15.64 \text{ m/s}$	$Cas_{mr} = 15.64 \text{ m/s}$	
6	$Cas_{me} = 11.92 \text{ m/s}$	$Cas_{me} = 11.92 \text{ m/s}$	
7	$\gamma_{bg} = -3.4484^\circ$	$\gamma_{bg} = -3.5819^\circ$	-
8	$Cd_{bg} = 0.02774$	$Cd_{bg} = 0.02774$	-
9	$Cl_{bg} = 0.46035$	$Cl_{bg} = 0.44315$	-
10	$D_{bg} = 4.7265 \text{ N}$	$D_{bg} = 1.1028 \text{ N}$	-
11	$L_{bg} = 78.4376 \text{ N}$	$L_{bg} = 17.6173 \text{ N}$	-
12	$D_{oc} = 5.4152 \text{ N}$	$D_{oc} = 1.2755 \text{ N}$	-
13	$P_{mr} = 74.188 \text{ W}$	$P_{mr} = 17.3094 \text{ W}$	-
14	$P_{me} = 67.0123 \text{ W}$	$P_{me} = 14.7591 \text{ W}$	-
15	$P_{oc} = 123.1382 \text{ W}$	$P_{oc} = 27.0984 \text{ W}$	-
16	$T = 348 \text{ min}$	$T = 108 \text{ min}$	-

## 6.2. Conceptual and experimental drone model dimensional analysis

This section analyses the dimensions of the UAV experimental and conceptual models in order to predict the relevance of the calculated parameters to the actual situation.

### *Dynamic similarity*

The dynamic similarity condition will then ensure that the load factor of the prototype will be equal to the load factor of the model. Mathematically, it is possible to calculate the speed in the wind tunnel,  $V_m$ , that is required to match the Reynolds number, and we can align the scale measurements of the lifting force from the test in the wind tunnel with the full-size prototype in the following way:

$$\alpha_m = \alpha_p \quad (6.1)$$

$$Re_m = \frac{\rho_m V_m c_m}{\mu_m} = Re_p = \frac{\rho_p V_p c_p}{\mu_p} \quad (6.2)$$

$$V_m = \frac{\rho_p c_p \mu_m}{\rho_m c_m \mu_p} V_p \quad (6.3)$$

$$\frac{L_p}{\rho_p V_p^2 c_p^2} = \frac{L_m}{\rho_m V_m^2 c_m^2} \quad (6.4)$$

$$L_p = \frac{\rho_p}{\rho_m} \left( \frac{V_p}{V_m} \right)^2 \left( \frac{c_p}{c_m} \right)^2 L_m \quad (6.5)$$

According to Eq. (6.3), the speed of the conceptual model, knowing the parameters of the experimental model (see Table 6.1), is as follows:

$$V_{km} = \frac{\rho_{em} \times c_{em} \times \mu_{km}}{\rho_{km} \times c_{km} \times \mu_{em}} \times V_{em} = \frac{1.184 \times 0.242 \times 1.802 \times 10^{-5}}{1.184 \times 0.3725 \times 1.802 \times 10^{-5}} \times 13.89 = 9.02 \frac{m}{s}, \quad (6.6)$$

until

$$V_{km} = \frac{1.184 \times 0.242 \times 1.802 \times 10^{-5}}{1.184 \times 0.3725 \times 1.802 \times 10^{-5}} \times 19.4 = 12.6 \frac{m}{s}. \quad (6.7)$$

And according to Eq. (6.5), the lift force of the conceptual model, knowing the parameters of the experimental model (see Table 6.2), is as follows:

$$L_{km} = \frac{\rho_{km}}{\rho_{em}} \times \left(\frac{V_{km}}{V_{em}}\right)^2 \times \left(\frac{c_{km}}{c_{em}}\right)^2 \times L_{em} = 17.602 \text{ N} \quad (6.8)$$

Comparing the data in Table 8.2 gives the following result:

$$L_{km} = \frac{1.184}{1.184} \times \left(\frac{15.8295}{14.9322}\right)^2 \times \left(\frac{0.3725}{0.242}\right)^2 \times 17.6173 = 46.908 \text{ N}, \quad (6.9)$$

which accounts for 40 % of error, that given the condition of geometric similarity, is possible.

In order to perform the test on the experimental model and to obtain data equal to the conceptual model, the flight condition for dynamic similarity shall be performed at the following speed according to Eq. (6.3):

$$V_{em} = \frac{\rho_{km} \times c_{km} \times \mu_{em}}{\rho_{em} \times c_{em} \times \mu_{km}} \times V_{km} = \frac{1.184 \times 0.3725 \times 1.802 \times 10^{-5}}{1.184 \times 0.242 \times 1.802 \times 10^{-5}} \times 15.8295 = 24.37 \frac{m}{s}, \quad (6.10)$$

which is practically impossible, as the maximum possible speed for the experimental model is set at 19.04 m/s (see Table 6.2).

In this way, the wind tunnel speed can be properly set to match Reynolds' number. After measuring the lifting force for the wing of the model,  $L_m$ , the lifting force for the prototype,  $L_p$  [59], [60], can be properly predicted (using Eq. (6.5)).

### ***The Buckingham Pi Technique***

#### ***Wing lifting capacity***

An incompressible flow over the wing of the aircraft is assumed. The capacity of the wing depends on the flow rate, the angle of attack, the length of the wing chord, and the density and viscosity of the liquid/gas. The analysis will be carried out using Buckingham's Pi Technique in the following six steps:

- Step 1.  $n$  – number of variables in the solution that is  $n = 6$ .

$$L = f(V, \alpha, c, \rho, \mu) \quad (6.11)$$

- Step 2. Dimensions for each variable.

Table 6.3

Variable Dimensions

Variable	Name	Dimension
$L$	lifting force	$M (L) (T^{-2})$
$V$	speed	$L (T^{-1})$
$C$	chord length	$L$
$\rho$	density	$M (L^{-3})$
$\mu$	viscosity	$M (L^{-1}) (T^{-1})$
$\alpha$	angle of attack	1 (dimensionless)

- Step 3. Finding  $j$ . First,  $j$  is taken;  $j$  – the number of primary dimensions in the solution. From the list above, mass, length, and time are the only primary dimensions in the list of original variables. Thus,  $j = 3$ . It expresses that  $k = n - j = 6 - 3 = 3$ . Three  $Pi$  from the dimensional analysis are expected.
- Step 4. Selecting repeating variables of  $j$ . You must now select 3 repeating variables. The lifting force is not a good choice because it is a dependent variable in this solution. The angle of attack is not allowed to be selected because it is already dimensionless (note that the angle of attack will be displayed as a dimensionless  $Pi$  by itself!). Of the remaining, viscosity is the least “baseline” or “desirable” variable to repeat across all  $Pi$  groups. Then the best choice in this case is density, speed and chord length.
- Step 5. Make up  $Pi$  groups. Taking the lifting force as the first, as it is the dependent variable,

$$\Pi_1 = LV^a c^b \rho^c \quad (6.12)$$

$$\{M^0 L^0 T^0\} = \left\{ \left( \frac{ML}{T^2} \right) \left( \frac{L}{T} \right)^a (L)^b \left( \frac{M}{L^3} \right)^c \right\} \quad (6.13)$$

$$\text{Equation of mass exponents: } 0 = 1 + c, \text{ or } \underline{c = -1.}$$

$$\text{Equation of time exponents: } 0 = -2 - a, \text{ or } \underline{a = -2.}$$

$$\text{Equation of length exponents: } 0 = 1 + a + b - 3c, \text{ or } \underline{b = -2.}$$

So,

$$\Pi_1 = \frac{L}{\rho V^2 c^2}. \quad (6.14)$$

Similarly, the second  $Pi$  group is composed using viscosity and repeating variables:

$$\Pi_2 = \mu V^e c^f \rho^g \quad (6.15)$$

$$\{M^0 L^0 T^0\} = \left\{ \left( \frac{M}{LT} \right) \left( \frac{L}{T} \right)^e (L)^f \left( \frac{M}{L^3} \right)^g \right\} \quad (6.16)$$

$$\text{Equation of mass exponents: } 0 = 1 + g, \text{ or } \underline{g = -1.}$$

$$\text{Equation of time exponents: } 0 = -1 - e, \text{ or } \underline{e = -1.}$$

$$\text{Equation of length exponents: } 0 = -1 + e + f - 3g, \text{ or } \underline{f = -1.}$$

So,

$$\Pi_2 = \frac{\mu}{\rho V c} \text{ or in a more appropriate way } \Pi_2 = \frac{\rho V c}{\mu}. \quad (6.17)$$

Note that this  $Pi$  group was inverted to match the more known dimensionless group of flow mechanics, *Reynolds number*. Mathematically, it wouldn't be wrong to be left upside down, but it is so to say “socially unacceptable” to do so.

- Step 6. Write the final functional relationship:

$$\frac{L}{\rho V^2 c^2} = f\left(\frac{\rho V c}{\mu}, \alpha\right) \quad (6.18)$$

Note that the previous dependent variable function of the solution from five independent variables is reduced to one dependent variable as a function from only two independent parameters. The dependent  $Pi$  group on the left side of the equation is the lift factor (usually multiplied by 2 for convenience), and the first independent parameter on the right side of the equation is *Reynolds number*, as mentioned above.

- Referring to the principle of dynamic similarity, in this solution, if a wing model is constructed on a geometric scale and it is tested at some angle of attack and some *Reynolds number*, the measured lift factor will surely be equal to the full-size prototype lift factor if applied at the same *Reynolds number* and the angle of attack.

Referring, as appropriate, to the principle of dynamic similarity and data from the experimental model, *Reynolds number* and drag force factor shall be:

$$R_{e_{em}} = \frac{\rho_{em} V_{em} c_{em}}{\mu_{em}} = \frac{1.184 \times 14.9322 \times 0.242}{1.802 \times 10^{-5}} = 237430, \quad (6.19)$$

$$C_{D_{em}} = \frac{D_{em}}{\rho_{em} V_{em}^2 c_{em}^2} = \frac{1.1028}{1.184 \times 14.9322^2 \times 0.242^2} = 0.071329. \quad (6.20)$$

Subsequently, the *Reynolds number* and the drag force factor of the conceptual model shall also be the same:

$$R_{e_{km}} = R_{e_{em}} = 237430 = \frac{\rho_{km} V_{km} c_{km}}{\mu_{km}}, \quad (6.21)$$

or

$$V_{km} = \frac{R_{e_{em}} \mu_{km}}{\rho_{km} c_{km}} = \frac{237430 \times 1.802 \times 10^{-5}}{1.184 \times 0.3725} = 9.7 \frac{\text{m}}{\text{s}}, \quad (6.22)$$

showing an error of 38 % in Table 8.2, and

$$C_{D_{km}} = C_{D_{em}} = 0.071329 = \frac{D_{km}}{\rho_{km} V_{km}^2 c_{km}^2}, \quad (6.23)$$

or

$$D_{km} = C_{D_{em}} \rho_{km} V_{km}^2 c_{km}^2 = 0.071329 \times 1.184 \times 15.8395^2 \times 0.3725^2 = 2.9364 \text{ N}, \quad (6.24)$$

which, as in the case of the  $V_{km}$  speed calculation, shows an error in the data in Table 6.2 of ~ 39 %. This, in turn, is possible on the basis of dynamic and geometric similarity, since the geometric similarity difference between the two models is 50 % (~ 1 : 2) and the difference between the other relevant parameters (mass, wing area, electric motor power) is 75 % (~ 1 : 4) [59], [60].

### 6.3. Scaled experimental model test un parameter identification in the wind tunnel

The wind tunnel is a tool for research and understanding aircraft performance, usually through experiments with a scaled model. Tests in the wind tunnel allow detailed characterization of the flow by measuring pressure, surface friction, speed and turbulence fields and other measurements. By applying appropriate measurement techniques, these parameters allow detailed estimation of numerical and analytical methods. Experiments in the wind tunnel allow the analysis of certain critical phenomena occurring at extreme conditions such as massive flow separation, volatility, flutter and others. These experiments may also involve detailed research of the local phenomena such as shock-wave/boundary-layer interactions, development of mixing zones, vortices, laminar to turbulent boundary-layer transition and others [61], [62].

A 3D printed UAV model was mounted on the laboratory wind tunnel (see Fig. 6.1).



Fig. 6.1. (a) – 3D printed in 10 % scale UAV model; (b) – printed model mounted on the wind-tunnel.

For the purpose of the experiment, the angle of attack  $\alpha$  variation from  $-10^\circ$  to  $30^\circ$  and a flow rate of  $V = 12$  m/s were taken. The results obtained should be summarized in a table.

Based on the results obtained, the  $C_L$  and  $C_D$  coefficient depending on the angle of attack  $\alpha$  variation graphs are constructed.

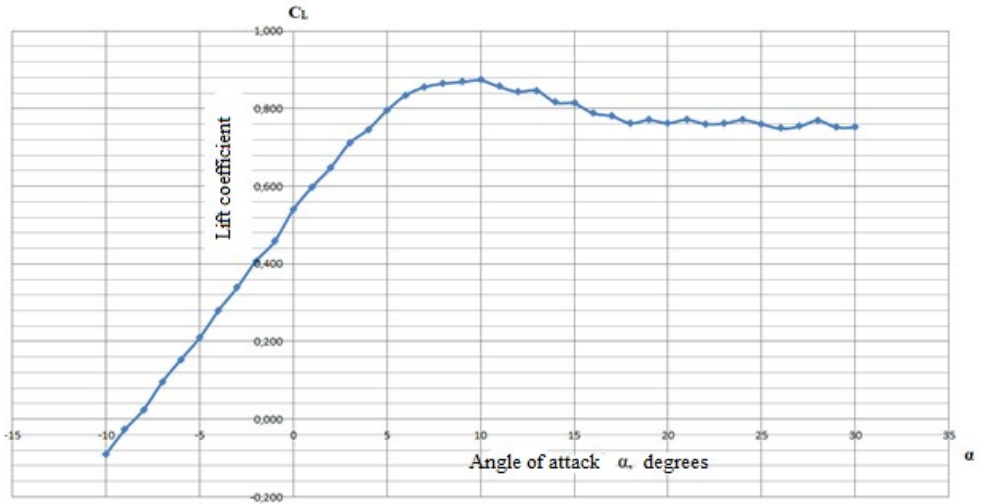


Fig. 6.2. Lift coefficient  $C_L$  vs the angle of attack  $\alpha$  variation graph.

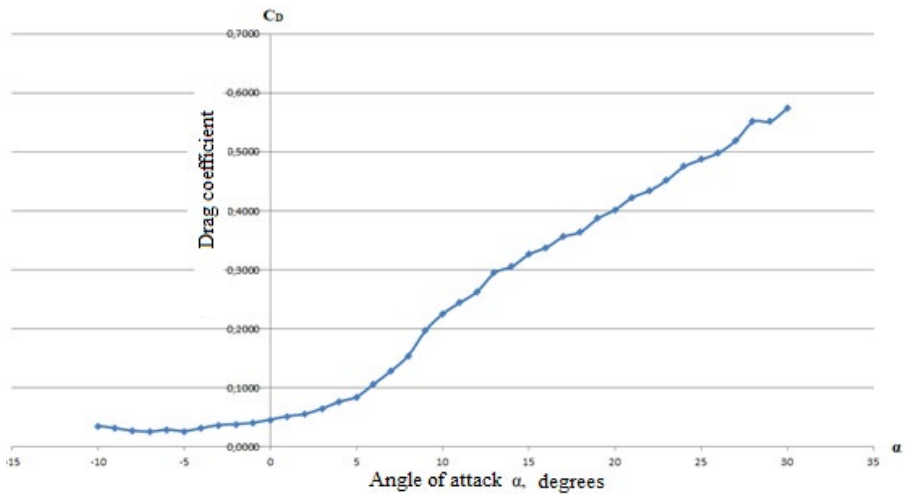


Fig. 6.3. Drag coefficient  $C_D$  vs the angle of attack  $\alpha$  variation graph.

As can be seen, the largest value of the  $L/D$  ratio is at the angle of attack  $\alpha$  value  $0^\circ$  in the experiment, which is the angle of attack of the whole model. But taking into account the wing's design setting angle  $\alpha_{set}$ , which is  $4.6^\circ$  for the wing inboard part and  $3.1^\circ$  for the wing outboard part, respectively, which was determined to obtain the maximum  $L/D$  ratio value, which provides the constructive requirement for maximum flight duration. As shown in Figs. 8 to 10, showing the variation of the lifting coefficient  $C_L$  to the angle of attack  $\alpha$ , the maximum  $C_L$  value is 0.874 at the angle of attack of  $10^\circ$ . Taking into account the angle of wing setting  $\alpha_{set} = 4.6^\circ$ , the overall angle of attack of the wing is  $14.6^\circ$ . The structural properties of the laboratory

wind tunnel cause an error in the angle of attack, increasing its value of  $\Delta\alpha$  by approximately  $5^\circ$ . Based on this error, the results correspond to the values obtained during the initial design process for the wing airfoil section selection.

#### **6.4. Chapter summary and conclusions**

This chapter examined the conformity of the conceptual model with the real-world requirements by using the dimensional analysis method and using the commercially available prototype of UAV model that is shown in Annex 18. The method of dimensional analysis showed that it can be successfully applied, but for accurate results, precise conceptual and experimental model dynamic similarity is required and should be established. In this case, significant accuracy could be obtained for parameters of the experimental model such as Reynolds number, lift factor and drag factor, provided that the experimental model's wing is manufactured on an exact geometrical scale against the conceptual design model wing and the same wing cross section shape.

## RECOMMENDATIONS FOR FURTHER RESEARCH

Conducting research in the field of unmanned aerial vehicle systems is difficult because the global progress of these systems is very rapid and versatile. Research in this area requires a significant contribution of funds, which is mainly limited to developed companies with already existing resources and profitable production infrastructure. A fully-fledged study in the field of unmanned aerial vehicle systems can be carried out if there is a well-functioning system that has already been developed and can then be carried out in some functional direction planned by the investigator concerned. A system flight functionality simulation program, which can first check the performance of the developmental, innovative system, which basically minimizes losses during development, which can take the form of a catastrophic landing of a drone and the destruction of relevant elements, is also usually provided to the relevant operating system. For the most part, researchers chose to conduct research on existing systems and provide a description and data on their performance. Some studies have investigated the performance of the unmanned aerial vehicles by landing with the deep stall method, provided data on the size of the touchdown path, vertical landing speed, but there are no data on the impact energy or force the unmanned aerial vehicle must absorb during the touchdown process. As part of the Thesis, in addition to existing systems already in use in commercially available unmanned aerial vehicle systems, the possibility of using the take-off and landing system of innovative unmanned aerial vehicles was considered, which, without the need for a large take-off and landing area, further provides a significantly reduced kinetic energy impact on the elements of the unmanned aerial vehicle during the landing touchdown process. Initially, a real experimental flight was conducted on a drone and landed with the proposed method of landing, introducing the drone into a controlled fall position, a subsequent twist, and approaching the Earth at approximately 3 m respectively, leading it out of the spin and into a controlled circular flight motion to the landing moment. The experimental research was conducted with a hand-held control radio-machine that cannot provide accurate results, but despite this, in the experiment phase, when the drone landed successfully, with the sequence of procedure described above, no visually identifiable damage was caused to its airframe. In addition to the study carried out, the development of a flight model in the simulation program (MATLAB) should still be carried out and the developed conceptual landing model integrated into the autopilot program of the unmanned system aircraft, which is the objective of further research.

Similarly, to address the existing problem in the field of drones, which limits the use of aircraft-type drones due to the run path required for existing drones in a straight linear direction, the Thesis proposes an innovative solution that solves this problem – the circular take-off system. As with the landing system, the experimental research was conducted with a hand-held radio controller that cannot provide accurate results, but despite this, during the experimental phases, the drone successfully continued the run-in phase (Annex 5) to take off, after the operator's orbital run-in phase. As before, in addition to the study carried out, the development of a flight model in the simulation program (MATLAB) should still be carried out and the developed conceptual take-off model integrated into the autopilot program of the unmanned system aircraft, which is the objective of further research. The theoretical calculations

demonstrate that landing the unmanned aerial vehicle in the proposed innovative manner significantly reduces the kinetic energy of the landing touchdown (Table 6.5) to be absorbed by the airframe of the unmanned aerial vehicle when touching the ground during the contact phase. Similarly, the take-off phase in the proposed innovative system requires a lower take-off rate.

A methodology was developed for the design of the flight load diagram of unmanned aerial vehicles (Annex 2), which allows the flight load diagram to be recreated in the design process of the aircraft itself to ensure that the design process is proceeding in the required direction and in accordance with the design requirements.

A methodology for obtaining basic data for the design of unmanned aerial vehicles (Annex 3) was developed by the *Matching Plot Technique*, which allows the acquisition of basic data (required wing area, engine power) of the unmanned aerial vehicle system for the subsequent construction process, as well as recalculation of data, if necessary, and the design process has deviated from the requirements and design objectives originally set.

In the Thesis, a drone system was developed in general, which by its performance exceeds the currently commercially available systems. The performance of the drone parameters was tested in the MATLAB simulation program and the performance results obtained meet the requirements originally set. In addition, a full-flight model development and simulation program (MATLAB) would still have to be carried out and the performance of the drone at different weather conditions tested. Following a full simulation test of the model, the program requires the development and verification of the real model under real conditions, which is the objective of future research.

Further research is needed to integrate innovative landing and take-off systems into a real model of the unmanned aerial vehicle system in automatic mode. There is a need to develop a system simulation model that could adapt them to different drone systems in the future, assess their use in different weather and terrain.

## CONCLUSIONS

1. The analysis of research and literature carried out in the field of unmanned aerial vehicles shows that experiments have been carried out only within existing systems and solutions, no experiments and research in the field of new development have been carried out. The studies conducted show data on the systems being used, which is also a good factor for use in comparing data to new development.
2. The method of selecting the type of unmanned aircraft used was based on the requirements laid down, allowing the parameters of the choice to be defined quantitatively, so that it was possible to select the most optimal model of aircraft on the basis of calculations.
3. The method of selecting the aircraft type could also be used to select all other elements of the unmanned aerial vehicle system in quantitative form based on calculations.
4. Practical flights conducted during the development process of the unmanned aerial vehicle system with a comparable model, enable new solutions to be found and the performance capabilities of the selected aircraft model to be understood. New solutions were found for launching and landing the drone, which ensure that they are launched and landed on a limited open area, as well as the landing process of the aircraft has significantly reduced (~ 80 %) impact kinetic energy to be absorbed by the air vehicle's airframe. A developed aircraft launch system ensures the launch of the aircraft on a restricted free area and is safe for the operator launching the aircraft.
5. The research methods and simulation programs used allow the accuracy of the system design process to be checked from the outset, which allows avoiding more problems and misunderstandings in future development steps. Simulation tools are an integral part of the construction process.
6. The development of the study and the UAV conceptual model made it possible to assess the technical and economic advantages of the lightweight or mini-category UAV aerodynamic scheme of the flying wing type with the conceptual development of landing and take-off systems as well as the small number of structural parts to be manufactured.
7. The study allows to explore various computer simulation programs and their practical application in the system development process, compare their performance, results, test the positive effects of winglets on aerodynamic properties of flying wing-type UAV at small Reynolds numbers.
8. The design process developed a method for constructing an aircraft flight envelope based on the MATLAB program. The aircraft's flight envelope is essential for ensuring its lifecycle. The flight envelope is recalculated multiple times during the construction process to ensure that the construction is performed in compliance with the safety requirements.
9. The design process developed a method for obtaining basic design parameters for the aircraft, which is the wing area and engine power of the drone, on the basis of the MATLAB program. The design parameters of the unmanned aerial vehicle are essential for the design process to go in the right direction, for no misunderstanding in the further design process and for achieving the design objectives. The method is based on the *Matching Plot Technique*.

## BIBLIOGRAPHY

- [1] Valavanis K. P., Vachtsevanos G. J., Handbook of Unmanned Aerial Vehicles. Springer, 2015.
- [2] Sadraey M. H., Design of Unmanned Aerial Systems. John Wiley & Sons, 2020.
- [3] Webster J. G., Eren H., Measurement, Instrumentation, and Sensors Handbook: Electromagnetic, Optical, Radiation, Chemical, and Biomedical Measurement. Taylor & Francis Group, 2014.
- [4] Kwon Y., Jinyeong H., Sekyung J., Seunghee Y., Suhwan K., Analysis of Design Directions for Ground Control Station (GCS). Journal of Computer and Communications, 2016.
- [5] Unmanned Systems Integrated Roadmap FY2013 – 2038.
- [6] European RPAS Steering Group. Roadmap for the integration of Civil Remotely-Piloted Aircraft Systems into the European Aviation System. 2013.
- [7] Peterson M. e., The UAV and the current and future regulatory construct for integration into the national airspace system.
- [8] Reg Austin, Unmanned Aircraft Systems: UAVS Design, Development and Deployment, First Edition. – New Jersey: John Wiley & Sons, 2010. – 332 pages.
- [9] Kimon P. Valavani, Advances in Unmanned Aerial Vehicles, Springer, 2007. – 543 pages.
- [10] Aksu, O., Alwardt, Ch., Bendsen, S., and others, A Comprehensive Approach to Countering Unmanned Aircraft Systems. Joint Air Power Competence Center. 2020. – 644 pages.
- [11] Joint Authorities for Rulemaking of Unmanned Systems: JARUS Guidance Material to JARUS-FCL Recommendation, WG1, Version 0.4, February 2017, JAR\_doc\_10, D.4.
- [12] Joint Authorities for Rulemaking of Unmanned Systems: Recommendations for Certification Specification for Light Unmanned Aeroplane Systems, WG-3 Airworthiness, Edition 0.3, November 2016, JAR\_DEL\_WG3\_D.04.
- [13] Joint Authorities for Rulemaking of Unmanned Systems: Recommendations for Certification Specification for Unmanned Aircraft Systems, WG-3 Airworthiness, Edition 1.0, September 2019, JARUS-DEL-WG3- CS-UAS-D.04.
- [14] Sadraey, M., Aircraft Design, John Wiley & Sons, Ltd, 2013.
- [15] Roskam, J., Airplane Design, DAR Corporation, 2003.
- [16] Torenbeek, E., Advanced aircraft design: Conceptual design, analysis and optimization of subsonic, civil airplanes, John Wiley & Sons, Ltd., 2013.
- [17] Stinton, D., The Design of the Aeroplane, AIAA, 2001.
- [18] Joint Authorities for Rulemaking of Unmanned Systems: RPAS C2 link Required Communication Performance (C2 link RCP) concept, WG5, Edition V1.0, May 2016, JAR\_doc\_13.
- [19] Joint Authorities for Rulemaking of Unmanned Systems: JARUS Recommendations on the use of Controller Pilot Data Link Communications (CPDLC) in the RPAS communications context, WG5, Edition V1.0, June 2016, JAR\_doc\_07.

- [20] J. Gundlach, *Designing Unmanned Aircraft Systems: A Comprehensive Approach*, American Institute of Aeronautics and Astronautics, Inc., 2021, 869 pages.
- [21] National Aeronautics and Space Administration, NASA Headquarters: *NASA Systems Engineering Handbook*, Washington, D. C. 20546, December 2007, NASA/SP-2007-6105 Rev1.
- [22] National Aeronautics and Space Administration, NASA Headquarters: *NASA Risk Management Handbook*, Washington, D. C. 20546, November 2011, NASA/SP-2011-3422 Version 1.0.
- [23] National Aeronautics and Space Administration Headquarters, Office of the Chief Engineer: *NASA Space Flight Program and Project Management Handbook*, Washington, D. C. 20546, September 2014, NASA/SP-2014-3705, ISBN: 978-0-9710327-3-6.
- [24] National Aeronautics and Space Administration, NASA Headquarters: *NASA Schedule Management Handbook*, Washington, D. C. 20546, March 2011, NASA/SP-2010-3403.
- [25] National Aeronautics and Space Administration: *NASA Work Breakdown Structure (WBS) Handbook*, Washington, D. C. 20546, January 2018, NASA/SP-2016-3404/REV1.
- [26] Blanchard, B. S. and Fabrycky, W. J., *Systems Engineering and Analysis*, Prentice Hall, 2013.
- [27] Joaquim R. R. A. Martins, Andrew B. Lambe, *Multidisciplinary Design Optimization: A Survey of Architectures*, AIAA, 2013.
- [28] Singiresu S. Rao, T., *Engineering Optimization: Theory and Practice*. John Wiley & Sons, Inc, 2009.
- [29] Daniel P. Raymer, *Doctoral Thesis: Enhancing Aircraft Conceptual Design Using Multidisciplinary Optimization*, Report 2002-2, May 2002, ISBN 91-7283-259-2.
- [30] *Certification Specifications, CS-VLA*, European Aviation Safety Agency, 2009, [www.easa.europa.eu](http://www.easa.europa.eu).
- [31] Sadraey, M., *Aircraft Performance Analysis*, VDM Verlag Dr. Müller, 2009.
- [25] Bertin, L. J. and Cummings, R. M., *Aerodynamics for Engineers*, 5th edn, Pearson/Prentice Hall, 2009.
- [32] Lan, E. C. T. and Roskam, J., *Airplane Aerodynamics and Performance*, DAR Corporation, 2003.
- [33] Roskam, J., *Airplane Flight Dynamics and Automatic Flight Control*, DAR Corporation, 2007.
- [34] McCormick, B. W., *Aerodynamics, Aeronautics and Flight Mechanics*, Wiley-VCH Verlag GmbH, 1979.
- [35] Etkin, B. and Reid, L. D., *Dynamics of Flight-Stability and Control*, 3rd edn, Wiley-VCH Verlag GmbH., 1996.
- [36] Martin Hepperle, <http://www.MH-AeroTools.de/>, 2006.
- [37] Mark D. Maughmer: *The Design of Winglets for Low-Speed Aircraft*, The Pennsylvania State University.

- [38] Saravanan Rajendran, Design of Parametric Winglets and Wing tip devices – A Conceptual Design Approach, Linkoping University, Institute of Technology, Department of Management and Engineering (IEI).
- [39] Phil R. Rademacher, Winglet Performance Evaluation Through The Vortex Lattice Method, Embry-Riddle Aeronautical University, Daytona Beach, Florida, May 2014.
- [40] Randal W. Beard, Timothy W. McLain, Small Unmanned Aircraft: Theory and Practice, the United Kingdom: Princeton University Press, 2012. – 317 pages.
- [41] David G. Hull, Fundamentals of Airplane Flight Mechanics, 4th edn, Springer-Verlag Berlin Heidelberg, 2007.
- [42] H. Taniguchi, Analysis of Deepstall Landing for UAV, The University of Tokyo, 26th International Congress of The Aeronautical Sciences, 2008.
- [43] Siri H. Mathisen, K. Grytey, Thor I. Fossen, Tor A. Johansen, Non-linear Model Predictive Control for Longitudinal and Lateral Guidance of a Small Fixed-Wing UAV in Precision Deep Stall Landing, Norwegian University of Science and Technology.
- [44] W. J. Crowther, K.Prassas, Post Stall Landing for Field Retrieval of UAVs, University of Manchester, 2023.
- [45] Pranav Jetley, P. B. Sujit, Srikanth Saripalli, Safe Landing of Fixed Wing UAVs, 47th Annual IEEE/IFIP International Conference on Dependable Systems and Networks Workshops, 2017.
- [46] Pointer W., Kotsis G., Langthaler P., Naderhirn M., Using formal methods to verify safe deep stall landing of a MAV, DOI: 10.1109/DASC.2011.6096086, 2011.
- [47] Gian-Andrea H., Optimizing Deep-stall Landing Maneuvers on Small Fixed-wing UAVs, ETH Library, 2019.
- [48] Siri M., Gryte K., Gros S., Johansen T. A., Precision Deep-Stall Landing of Fixed-Wing UAVs using Nonlinear Model Predictive Control, Norwegian University of Science and Technology, 2010.
- [49] Aviation Education. [www.luizmonteiro.com](http://www.luizmonteiro.com).
- [50] J. Kirtley, Electric Motor Handbook, McGraw-Hill ([www.digitalengineeringlibrary.com](http://www.digitalengineeringlibrary.com)), 2004.
- [51] Mclean, D., Automatic Flight Control Systems, Prentice-Hall, 1990.
- [52] Nelson, R., Flight Stability and Automatic Control, McGraw Hill, 1989.
- [53] Doug Griffith, General Image Quality Equation (GIQE), National Geospacial-Intelligence Agency, JACIE Conference, 18 April 2012.
- [54] G. M. Koretsky, J. F. Nicoll, M. S. Taylor, A Tutorial on Electro-Optical/Infrared (EO/IR) Theory and Systems, Institute for Defense Analyses, IDA Document D-4642, January 2013.
- [55] Jingbo Bai, Yangyang Sun, EO Sensor Planning for UAV Engineering Reconnaissance Based on NIIRS and GIQE, Hindawi, Mathematical Problems in Engineering, Volume 2018, Article ID 6837014, 9 pages.

- [56] Mary A. Lumang, Long-Range Surveillance Cameras & Johnson's Criteria, [www.cohu-cameras.com](http://www.cohu-cameras.com).
- [57] Anderson, J., Introduction to Flight. McGraw Hill Education, 2016, 929 pages.
- [58] <https://www.mathworks.com>.
- [59] B. Zohuri, Dimensional Analysis and Self-Similarity Methods for Engineers and Scientists, Springer International Publishing Switzerland, 2015, 379 pages.
- [60] Frank M. White, Fluid Mechanics, 8<sup>th</sup> Edition, McGraw-Hill Education, 2016, 780 pages.
- [61] S. Discetti, A. Ianiro, Experimental Aerodynamics, Taylor & Francis Group, 2017, 483 pages.
- [62] B. Chanetz, J. Délery, P. Gilliéron, P. Gnemmi, E.R. Gowree, P. Perrier, Experimental Aerodynamics: An Introductory Guide, Springer Tracts in Mechanical Engineering, 2020, 329 pages.



**Nikolajs Glīzde** was born in 1966 in Riga. In 1993 he obtained a Bachelor's degree in Engineering Sciences from Riga Technical University, and in 1994 he obtained the qualification of mechanical engineer. In 2011, he received a Master's degree in Transport Systems Engineering. He served in the National Armed Forces from 2002 till 2022. Since 2016, he has been a lecturer and researcher at Riga Technical University. His scientific interests are related to aviation, technology and transport.